


MUFASA: The strength and evolution of galaxy conformity in various tracers

Mika Rafieferantsoa^{1,2,3} *, Romeel Davé^{5,1,3,4}

¹ University of the Western Cape, Bellville, Cape Town 7535, South Africa

² Max-Planck-Institut für Astrophysik, Garching, Germany

³ South African Astronomical Observatory, Observatory, Cape Town 7925, South Africa

⁴ African Institute for Mathematical Sciences, Muizenberg, Cape Town 7945, South Africa

⁵ Institute for Astronomy, Royal Observatory, Edinburgh EH9 3HJ, UK

Last updated 2017 December 18; in original form 2017 July 6

ABSTRACT

We investigate galaxy conformity using the MUFASA cosmological hydrodynamical simulation. We show a bimodal distribution in galaxy colour with radius, albeit with too many low-mass quenched satellite galaxies compared to observations. MUFASA produces conformity in observed properties such as colour, sSFR, and HI content; i.e. neighbouring galaxies have similar properties. We see analogous trends in other properties such as in environment, stellar age, H₂ content, and metallicity. We introduce quantifying conformity using $\mathcal{S}(R)$, measuring the relative difference in upper and lower quartile properties of the neighbours. We show that low-mass and non-quenched haloes have weak conformity ($\mathcal{S}(R) \lesssim 0.5$) extending to large projected radii R in all properties, while high-mass and quenched haloes have strong conformity ($\mathcal{S}(R) \sim 1$) that diminishes rapidly with R and disappears at $R \gtrsim 1$ Mpc. $\mathcal{S}(R)$ is strongest for environment in low-mass haloes, and sSFR (or colour) in high-mass haloes, and is dominated by one-halo conformity with the exception of HI in small haloes. Metallicity shows a curious anti-conformity in massive haloes. Tracking the evolution of conformity for $z = 0$ galaxies back in time shows that conformity broadly emerges as a late-time ($z \lesssim 1$) phenomenon. However, for fixed halo mass bins, conformity is fairly constant with redshift out to $z \gtrsim 2$. These trends are consistent with the idea that strong conformity only emerges once haloes grow above MUFASA’s quenching mass scale of $\sim 10^{12} M_{\odot}$. A quantitative measure of conformity in various properties, along with its evolution, thus represents a new and stringent test of the impact of quenching on environment within current galaxy formation models.

Key words: galaxies: evolution – galaxies: formation – galaxies: statistics – methods: N-body simulations

1 INTRODUCTION

Environment plays an important role in setting the properties of galaxies. The collapse of massive haloes and large filaments results in the shock heating of gas, which inhibits the growth of galaxies within these structures by a combination of strangulation (or starvation), ram pressure stripping, and tidal stripping. These environmental processes connect the physics of intergalactic gas and large-scale structure with the observable stellar properties of galaxies,

and hence represent a key test for cosmologically-situated galaxy formation models.

A particular phenomenon that has gained attention recently is the tendency for galaxies spatially close to each other to have similar galaxy colours. This was first noted in Weinmann et al. (2006) and given the name *galactic conformity*. They used a galaxy sample from the Sloan Digital Sky Survey (York et al. 2000, SDSS) and found that early-type central galaxies have comparatively higher fractions of early-type satellite galaxies around them, while late-type centrals tended to be surrounded by late-type satellites. Furthermore, the overall fractions of early and late types depended strongly on the mass of their respective haloes. This type of

* Contact e-mail: rafieferantsoamika@gmail.com

† South African Astronomical Observatory, Observatory Road, Cape Town 7925, South Africa

conformity was later dubbed “one-halo” conformity, since it quantifies the level of similarity within a single halo.

Conformity can arise owing purely to large-scale structure heating, because of the tendency of deep potential wells to shock-heat gas to high temperatures (e.g. [White & Rees 1978](#)). Such shock-heated gas is expected to surround galaxies in haloes with masses above $\sim 10^{12} M_{\odot}$ ([Birnboim & Dekel 2003](#); [Kereš et al. 2005](#); [Gabor et al. 2010](#)), and is likely related to the oft-mentioned bimodal distribution in galaxies properties (e.g. [Kauffmann et al. 2003](#); [Baldry et al. 2004](#)). Such bimodality is present in both central and satellite galaxy samples. This encompassing hot halo can thus naturally give rise to a correspondence between central and satellite star formation rates and gas contents.

But such a hot halo is not stable. The hot gas in the dense central region is expected to cool quickly, leading to substantially star formation in massive galaxies, in disagreement with observations. Thus most galaxy formation models introduce some feedback mechanism ([Somerville & Davé 2015](#)), putatively from the central active galactic nucleus (AGN), that maintains the hot hydrostatic halo ([Croton et al. 2006](#)). This same “maintenance mode” feedback can attenuate the star formation in satellite galaxies as well (e.g. [Ann et al. 2008](#); [Gabor & Davé 2012](#)). Hence one-halo conformity may encode information both about large-scale structure as well as AGN feedback processes in more massive systems.

[Kauffmann et al. \(2013\)](#) re-analysed galactic conformity in SDSS with a more rigorous sample selection, and found that moderate-mass central galaxies show galactic conformity out to distances that are many times their virial radius, as much as 4 Mpc, which has come to be called two-halo conformity since it corresponds to properties being similar in galaxies living in different haloes. In contrast, more massive centrals only show conformity to the neighbours within about a virial radius. To explore the physical origin of conformity, [Kauffmann \(2015\)](#) further found that central galaxies with low star formation rate are more likely to be located in a neighbourhood with higher fraction of massive galaxies that have active AGN, suggesting that AGN feedback plays a significant role in conformity.

However, the strength or perhaps even the existence of two-halo conformity is controversial. Recent work by [Tinker et al. \(2017\)](#) suggested that the large spatial extent of galactic conformity found in [Kauffmann et al. \(2013\)](#) may be the result of misclassifications of central galaxies, and that conformity beyond at most a Mpc disappears when the central sample is more carefully selected using a group catalog rather than projected distance. This is supported by [Sin et al. \(2017\)](#), who further showed that the strong two-halo conformity signal found by [Kauffmann et al. \(2013\)](#) can be reproduced with their semi-analytic model when using Kauffmann et al.’s selection, but when true central galaxies are used, the two-halo term is very weak and essentially undetectable in the SDSS data.

Conformity analogously appears in the neutral hydrogen content of galaxies. Using 40 galaxies from the Bluedisk project, [Wang et al. \(2015\)](#) found that galaxies with high HI fraction live in the vicinity of other galaxies with high HI fraction. Also, conformity persists out to higher redshift. [Hartley et al. \(2015\)](#) studied the satellite galaxies

drawn from the UKIRT Infrared Deep Sky Survey (UKIDSS [Lawrence et al. 2007](#)) and concluded that passive galaxies are more likely to be around passive galaxies with 3σ significance and that happens out to $z \gtrsim 2$. Using a set of satellite galaxies data from ZFOURGE ([Straatman et al. 2014](#)), UDS, and UltraVISTA ([McCracken et al. 2012](#)), [Kawinwanichakij et al. \(2016\)](#) looked at the evolution of galactic conformity and confirmed a one-halo conformity signal with a significance of more than 3σ out to $z \sim 1.6$, and a lower but noticeable signal out to $z \sim 2.5$. Similarly, [Berti et al. \(2016\)](#) investigated one- and two-halo conformity with the Primus survey (conducted with IMACS; [Bigelow & Dressler 2003](#)) data which they claimed to be uniquely suited due to large survey area of $\sim 9 \text{ deg}^2$ and redshift precision of $\sigma_z = 0.005(1+z)$. They detect more than 2.5σ one-halo conformity out to $z \sim 1$. They also found a hint at a two-halo conformity signal from the fact that central galaxies are more likely to be quiescent when they are located in dense environment. [Hatfield & Jarvis \(2016\)](#) used a different method by looking at the cross-clustering of galaxies with the 2-point correlation function and claim that specific star formation rate (sSFR)-density relation, which is another way of characterising conformity, emerges at $z \sim 1$ and keeps growing until today. Hence, it appears that conformity is a real effect not only in present-day galaxy colours, but in gas content at least, as well as to higher redshifts, though the precise strength and evolution depends on the sample selection and technique used to quantify conformity.

Given the emergence of this wealth of data on galaxy conformity, there has been various attempts to explain conformity within a hierarchical structure formation paradigm. [Hearin et al. \(2015\)](#) used semi-analytic models on the Bolshoi simulation ([Klypin et al. 2011](#)) and found that using either $M_{\text{halo, vir}}$ -based quenching prescription or a delayed-then-rapid quenching of the galaxies displayed zero conformity, while only their *age matching* model showed statistically significant galactic conformity. This led them to conclude that two-halo conformity is the result of the central galaxy assembly bias. [Hearin et al. \(2016\)](#) followed up by looking at the assembly histories of structures and found that haloes separated with more than tens of their virial radius are connected because they are situated within the same large-scale tidal environment which is the main driver of their growth. However, [Zu & Mandelbaum \(2017\)](#) used a colour-based halo occupancy model to argue that (weak) large-scale conformity can arise purely from the environmental dependence of the halo mass function, without requiring any assembly bias. They also confirm the result of [Sin et al. \(2017\)](#) and [Tinker et al. \(2017\)](#) that the strong two-halo conformity seen by [Kauffmann et al. \(2013\)](#) is primarily an artifact of mis-identified central vs. satellite galaxies.

Modern cosmological hydrodynamic simulations include all the relevant effects that are expected to give rise to galactic conformity. Such models should, in principle, implicitly include halo assembly bias, halo occupancy evolution, and any correlations between the colours of centrals and satellites arising from included feedback processes, and hence galaxy conformity should be an emergent property. Such simulations track gas and star formation properties directly as well, so can be used to study conformity in various tracers, as well as their evolution with redshift. Nonetheless, as shown in e.g. [Gabor & Davé \(2015\)](#), the quenching of

satellites along with surrounding “backsplash” and “neighbourhood quenched” galaxies is dependent on the model for central galaxy quenching, which is at present not well constrained in galaxy formation models, and is typically included only in a prescriptive or heuristic manner. Hence it is instructive to examine conformity predictions from cosmological hydrodynamic simulations, and compare them to present and future observables as a detailed test of quenching models.

To this end, [Bray et al. \(2016\)](#) used the Illustris Simulation ([Vogelsberger et al. 2014](#)) to explore whether assembly bias can be an explanation for galaxy conformity. They found evidence of galactic conformity out to 10 Mpc for the smallest centrals, decreasing in strength with increasing stellar mass of the centrals. They developed a simple model based on abundance and age matching that was able to reproduce this signal, demonstrating that the galaxy colour-age relation is important for conformity.

In this paper, we use the MUFASA simulation ([Davé et al. 2016](#)) to study conformity. Our goal is to investigate conformity in a wide variety of galaxy tracers, to understand which galaxy and environmental parameters show the strongest levels of conformity, and to make predictions for conformity that can be used as a test of models. This differs in aim from previous works discussed above that have focused more on developing halo-based models for the origin of conformity, comparing to the (sparse) available data. We show that MUFASA predicts a conformity signal that is strongly dependent on halo mass, and that this signal is not limited to colour and neutral hydrogen but appears in many other galaxy properties as well. We propose a measure to quantify the strength of conformity and study its evolution in various tracers as a function of redshift. Our results indicate that galaxy conformity is a generic emergent feature of hydrodynamic galaxy formation models, and that the strength of conformity can be a valuable test of the interplay between environment, galaxy assembly, and feedback processes particularly related to quenching.

§2 briefly reviews the MUFASA simulation used for this work. In §3, we look at the satellite galaxy properties from our simulation. §4 expands on the comparison of conformity between our simulated galaxy sample and the observed data. §5 characterises the nature of conformity comparing between various tracers, and study its evolution out to intermediate redshifts. We summarize our conclusions in §6.

2 SIMULATIONS

2.1 Models

For this work we employ the MUFASA simulation, which is fully described in [Davé et al. \(2016\)](#). Here, we briefly review the main ingredients, and expound on the key physical aspects of MUFASA that are particularly relevant for this work.

MUFASA employs the GIZMO cosmological hydrodynamic code, including a tree-particle-mesh gravity code based on GADGET ([Springel 2005](#)), and a meshless finite mass hydrodynamic algorithm ([Hopkins 2015](#)). For radia-

tive processes, MUFASA utilises the GRACKLE 2.1 library¹ to cool the gas elements, accounting for non-equilibrium ionisation for primordial elements, as well as metal-line cooling assuming ionisation equilibrium, plus photoionisation heating computed with a spatially-uniform metagalactic flux taken from [Faucher-Giguère et al. \(2010\)](#). Star formation occurs in molecular gas, and only in gas elements with hydrogen number density $n_H \geq 0.13 \text{ cm}^{-3}$, with the star formation rate computed following a [Schmidt \(1959\)](#)-law scaling, namely

$$\text{SFR} = \varepsilon f_{\text{H}_2} G^{-0.5} \rho_{\text{gas}}^{0.5}. \quad (1)$$

Here ρ_{gas} is the density of the gas, $\varepsilon = 0.02$ ([Kennicutt 1998](#)) is the star formation efficiency, G the gravitational constant, and f_{H_2} the molecular hydrogen fraction in the gas element computed via a subgrid prescription from [Krumholz & Gnedin \(2011\)](#).

We assume that star formation in the simulation produces a combination of radiation pressure and supernovae energy which manifests by kicking out its surrounding gas volume elements at a given rate η relative to the star formation rate. Each outflowing wind element is ejected away from its host galaxy and in a direction perpendicular to the (\vec{v}, \vec{a}) plane with a launching wind velocity v_w , where \vec{v} and \vec{a} are the velocity and the acceleration of the gas cloud prior to its launch. To choose the free parameters, we take scaling relations from [Muratov et al. \(2015\)](#) based on the Feedback in Realistic Environments (FIRE) simulations. In particular, we choose the mass loading factor η and the wind speed v_w as follows:

$$\eta = 3.55 \left(\frac{M_*}{10^{10} M_\odot} \right)^{-0.35}; \quad (2)$$

$$v_w = 2v_c \left(\frac{v_c}{200 \text{ km s}^{-1}} \right)^{0.12}. \quad (3)$$

M_* and v_c are the stellar mass and circular velocity of the galaxy where the gas volume element is located. Galaxies are identified using an approximate on-the-fly friends-of-friends group finder specifically designed to be computationally fast and tuned to reproduce the same results as SKID² (Spline Kernel Interpolative Denmax); this is applied only to star-forming gas elements and stars.

Particularly relevant for this paper is that MUFASA includes an observationally motivated heuristic prescription to quench massive galaxies. Gas elements sitting in a host halo above a threshold quenching mass M_q are heated to around the virial temperature of that host. This is done except for the interstellar medium gas defined to have more than 10% neutral hydrogen fraction. The host halo is grouped on the fly with a (separate) friends-of-friends algorithm using a linking length of 0.16 times the mean inter-particle distance, including dark matter, gas, and stars. The virial temperature is taken to be $T_{\text{vir}} = 9.52 \times 10^7 M_h^{2/3}$ ([Voit 2005](#)). M_q is taken to be redshift dependent, whose scaling is taken from the analytic equilibrium model of galaxy formation ([Mitra et al. 2015](#)), who obtained a best-fit scaling of $M_q = (0.96 + 0.48z) \times 10^{12} M_\odot$.

¹ <https://grackle.readthedocs.io/en/grackle-2.1/genindex.html>

² <http://www-hpcc.astro.washington.edu/tools/skid.html>

Our sample from skid does not contain dark matter depleted galaxy (see Figure 1).

We note that this quenching prescription is purely heuristic, and is not a physical model for AGN feedback. It is specifically designed to mimic the effects of radio mode feedback (Croton et al. 2006) from active galactic nuclei (AGN), in which jets from the central galaxies of massive haloes are observed to add enough energy into diffuse gas to counterbalance cooling (McNamara & Nulsen 2007), without a detailed physical model for the AGN energy couples to the halo gas. Since we keep ambient gas hot all the way out to the virial radius in massive haloes, this feedback model can be regarded as a rather extreme form of maintenance mode quenching. In Davé et al. (2017a) we have showed that it results in a population of quenched central galaxies that is in reasonable agreement with key observations such as the colour-magnitude diagram of galaxies, although it appears to overproduce quenched satellite galaxies at low masses. The results on conformity here should be taken with these caveats in mind, noting that a different or more physical quenching model may yield different results.

2.2 Galaxy sample and operational definitions

The galaxy sample used for our analysis is obtained by simulating a cube of $50h^{-1}\text{Mpc}$ on a side with 512^3 dark matter particles and 512^3 gas volume elements. The initial conditions are generated at redshift $z = 249$ using MUSIC (Hahn & Abel 2011) with Planck et al. (2016)-concordant cosmological parameters, namely $\Omega_m = 0.3$, $\Omega_\Lambda = 0.7$, $\Omega_b = 0.048$, $H_0 = 68 \text{ km s}^{-1} \text{ Mpc}^{-1}$, $\sigma_8 = 0.82$ and $n_s = 0.97$. We also consider a $25h^{-1}\text{Mpc}$ volume with the same number of particles and the same input physics and cosmology, having a factor of 8 better in mass resolution, in order to assess resolution convergence.

MUFASA evolves these initial conditions to $z = 0$ outputting 135 snapshots. For each snapshot, we identify galaxies, with SKID² (Kereš et al. 2005), as gravitationally bound collections of stars and star-forming gas. For galaxy mass resolution, we take $5.8 \times 10^8 M_\odot$, where it was shown that the stellar mass functions converge with that limit (Davé et al. 2016). While this does not guarantee convergence in other properties such as colour, we will compute conformity using galaxies with $M_* > 1.8 \times 10^9 M_\odot$, three times larger than our nominal mass resolution and corresponding to approximately 100 star particles at minimum. Host haloes are identified using the friends-of-friends algorithm with a linking length of 2% the mean inter-particle distance. The galaxies are assigned to host haloes based on their spatial location. The most (stellar) massive galaxy in a given halo is considered as the central (regardless of physical location) and the remainder are satellites.

Figure 1 shows the stellar-to-halo mass ratio in central galaxies as a function of stellar mass, colour-coded by specific SFR. This shows that quenching kicks in rather rapidly at $M_* \gtrsim 10^{10.5} M_\odot$, above which the typical halo mass lies in the regime where MUFASA’s halo quenching model kicks in. There are a handful of galaxies with high M_*/M_{halo} ratios at lower masses, which tend to be quenched; these are typically former satellites whose orbits have taken them outside their host haloes (Gabor & Davé 2015), and thus have had their own haloes significantly impacted by stripping. Such galaxies should also appear in observational samples, and indeed there is strong increase in the passive fraction of galaxies

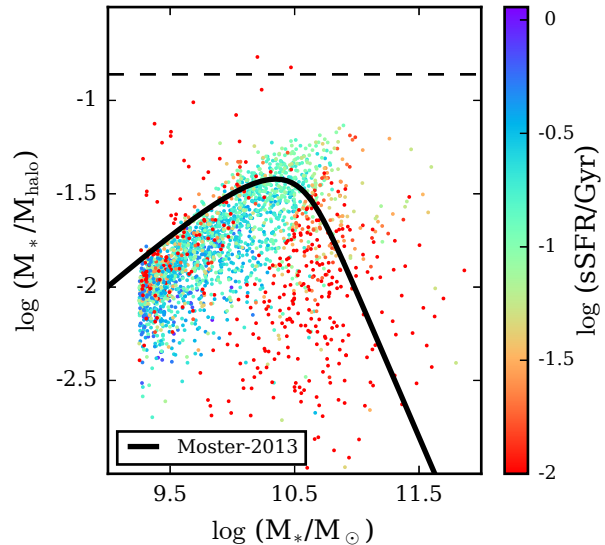


Figure 1. Stellar-to-halo mass ratio as a function of M_* for central galaxies in MUFASA. The ratio peaks around $M_* \sim 10^{10.5} M_\odot$ at around 25% of the cosmic baryon fraction (shown as the horizontal dotted line), dropping away quickly to higher and lower masses. The solid line shows the fit from abundance matching of observed galaxies by Moster et al. (2013); the predicted values are generally consistent with this.

lying close to but still outside the virial radius of massive galaxies (Geha et al. 2012). These have only a small impact on the overall conformity statistics.

The properties of these galaxies and haloes are calculated with a modified version of CAESAR³, which is an add-on package for the Yt simulation analysis suite. The stellar mass (M_*) of a galaxy is obtained by summing the masses of all its stellar particles, and we define the galaxy’s age as the time when half of these stars were formed. The galaxy star formation rate (SFR) is the summation of the instantaneous SFR of the gas elements (directly obtained from the simulation). The molecular hydrogen fraction (f_{H_2}) is the total mass of H_2 from all the gas elements, which is tracked directly in the simulation, divided by its stellar mass. The atomic hydrogen (HI) content of the galaxy is the aggregate amount of all HI from the gas particles. Before summing over, the gas HI mass from the simulation is post-processed to account for the self-shielding from the metagalactic UV background radiation, by using the fitting formula for the effective optically-thin photoionization rate as a function of density taken from Rahmati & Schaye (2014, see eq. 1). The HI richness (f_{HI} , or HI fraction) is the total HI content of the galaxy divided by its stellar mass M_* . To quantify the environment, we use the projected nearest neighbour density Σ_3 :

$$\Sigma_3 = \frac{3}{\pi R_3^2} \quad (4)$$

where R_3 is the distance of the galaxy to its 3rd closest neighbour, projected along the z-axis.

The colours of the galaxies are obtained using the

³ <https://bitbucket.org/laskalam/caesar>

LOSER⁴ package. Stellar spectra are interpolated from the age and the metallicity of star particles using the Flexible Stellar Population Synthesis (FSPS; Conroy & Gunn 2010) library. The metal column density is calculated along each line of sight, converted into a dust extinction, then applied to each star particle’s spectrum. The spectra of all the stars in each galaxy (from SKID) are then summed and the appropriate filter applied to get the magnitudes. See Davé et al. (2017a) for further details.

To analyse conformity, we follow the general procedure outlined in Kauffmann et al. (2013). First we subdivide our $z = 0$ central galaxies into three stellar mass bins: $\log(M_{*,\text{cen}}/M_{\odot}) \in \{[9.5, 10], [10, 10.5], [10.5, 11.5]\}$. The numbers of galaxies in each bins are 747, 587, and 561, respectively. We choose 10.5 – 11.5 for the largest bin (instead of 11 – 11.5 that was used in Kauffmann et al. 2013) because using smaller bin results in considerable shot noise owing to small numbers of such galaxies in our simulation; we checked that the results for our larger bin are consistent with that obtained from using only $M_* > 10^{11}M_{\odot}$, as both predominantly live in quenched haloes.

Within each stellar mass bin, we order the central (or primary) galaxies by a given property: colour, sSFR or HI richness (M_{HI}/M_*). We then take the objects at the lowest and the highest quartiles (< 25% and > 75%), and examine the median properties of neighbours of these galaxies as a function of radius out to 4 projected Mpc. Throughout our analysis, we employ jackknife resampling among 8 simulation sub-octants to estimate our errors.

Guided by the completeness level in the SDSS-based sample of Kauffmann et al. (2013), we only consider satellite galaxies with $M_* \geq 10^{9.25}M_{\odot}$, comfortably above our stellar mass resolution limit. However, unlike Kauffmann et al. (2013), we use friends-of-friends identified central galaxies instead of adopting their isolation criteria. This is more closely aligned with more recent analyses that use group catalogs, which has been shown to provide a more robust measure of conformity, particularly two-halo conformity, compared to the Kauffmann et al. isolation criterion (Tinker et al. 2017).

Figure 2 illustrates the difference in mass ratio of identified centrals to their neighbouring galaxies located within 500 projected kpc and 500 km s^{-1} redshift distance, which corresponds to the Kauffmann isolation criterion. The distribution of galaxies in the upper and lower quartiles in galaxy colour (top row), HI fraction (middle), and sSFR (bottom) are indicated in red and blue histograms, in three central mass bins (left to right columns). The numbers on the bottom right show the number of central galaxies in the respective stellar mass bin. This shows that overall a small fraction of the neighbours have $M_* > 0.5 \times M_{\text{primary}}$ (filled part of the histograms) where their respective central galaxies would not have been classified as isolated with respect to Kauffmann criteria. Given the relatively modest fraction of such neighbours ($\sim 15\%$) our conformity should be a robust prediction independent of isolation criterion, but for high-mass systems there will be systematic differences. Note that if we only used the satellite galaxies (not shown), the fraction

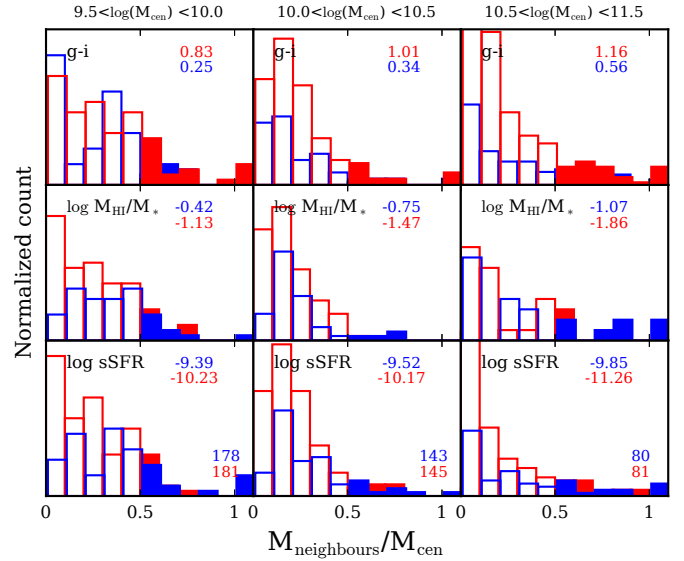


Figure 2. Stellar mass fraction of the neighbours relative to their respective central galaxies in our simulated box. We only show galaxies that are within 500 kpc projected distance and 500 km s^{-1} redshift distance from their primaries. The histograms at > 0.5 are filled to emphasize on the fractions of neighbours where their respective central galaxies would not have been classified as isolated galaxies if Kauffmann criteria were applied.

of neighbours with $M_* > 0.5 \times M_{\text{primary}}$ drops significantly to $\sim 5\%$. We will therefore compare to the Kauffmann et al. (2013) data for illustrative purposes only, with the caveat that the isolation criterion can play some role in the outcome.

3 SATELLITE GALAXY PROPERTIES IN MUFASA

Conformity is a measure of the environmental impact on galaxy formation. Hence it is important to ensure that environmental processes are reasonably accurately modeled in our simulation. As a test of this, we begin by presenting an analysis of the satellite galaxy population predicted in MUFASA.

3.1 Satellite versus central mass functions

Figure 3 shows the GSMF of the MUFASA simulated galaxies (black long-dashed lines): separated into central (brown dashed-dotted lines) and satellite (green dotted lines) galaxies at $z = \{0, 1, 2\}$. Observational data from Baldry et al. (2012) for $z = 0$ and Tomczak et al. (2014) for $z = \{1, 2\}$ are shown with the black circles.

As discussed in Davé et al. (2016), MUFASA reproduces the observed total GSMF and its evolution out to high redshifts fairly well, albeit with a modest excess at $z \sim 1$. The massive end of the GSMF consists almost entirely of central galaxies across all redshifts explored here. The contribution from the satellites is present only at the low mass

⁴ Line Of Sight Extinction by Ray-tracing <https://bitbucket.org/romeeld/closer>

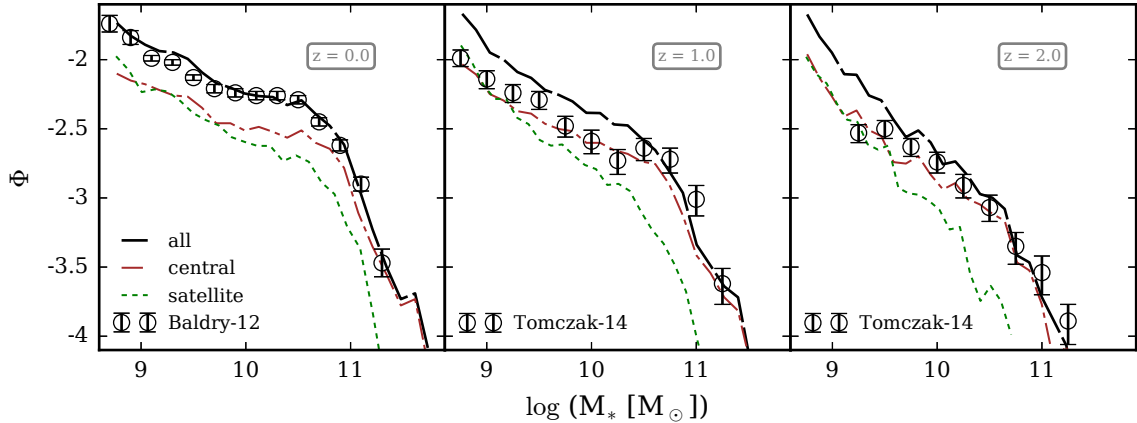


Figure 3. Galaxy stellar mass functions (black long-dashed lines) separated into central (brown dashed-dotted lines) and satellite (green dotted lines), at redshift $z = 0$ (left), $z = 1$ (middle) and $z = 2$ (right). At all epochs, central galaxies dominate by number at $M_* \gtrsim 10^{9-9.5} M_\odot$, and a knee begins to appear in the satellite mass function at $z \lesssim 1$. Observations of the total GSMF are shown with the black circles.

end ($M_* \lesssim 10^{9.5} M_\odot$) and it is modestly stronger at lower redshift.

Already at $z = 2$, the central GSMF starts to produce the knee while the satellite galaxies only show a hint of a knee at $z \lesssim 1$. The knee in GSMF is the result of an enhancement in star formation due to an increased contribution of wind recycling to higher masses (Oppenheimer et al. 2010), combined with the truncation of star formation in massive galaxies owing to our quenching prescription mimicking AGN feedback. At later epochs, the most massive satellites were until recently central galaxies that were massive enough to experience quenching, and hence they reflect a truncated high-mass GSMF of the centrals.

3.2 Star-forming versus quiescent satellite mass functions

Figure 4 breaks down the GSMF in terms of satellites split into star-forming and quiescent within four central galaxy stellar mass bins, following the same exercise as in Tal et al. (2014) using UltraVista data. Here we consider galaxies to be quiescent if $\log(\text{sSFR}/\text{Gyr}^{-1}) \leq -2.2$. In accordance with Tal et al. (2014), we define Φ to be the number of galaxies per group. In other words, for the sample of all the N central galaxies within a given stellar mass bin, Figure 4 shows the distribution of their satellite galaxies normalized by N . In their analysis, Tal et al. (2014) defined galaxies to be central if no other more massive galaxy could be found within two projected virial radii, which is broadly consistent with our definition to be the most massive galaxies in their respective haloes (see sec. 2.2). They consider all non-central galaxies within two virial radii of the central galaxies to be their satellites.

The total predicted satellite GSMF, as indicated by the thick solid grey lines, are in general agreement with the Tal et al. (2014) observational data shown by the thick dashed grey lines. There is a clear trend of a higher mass function of satellites around more massive centrals. The only notable discrepancy is that the observations show up to $\sim \times 2$ more satellites at intermediate masses in the

$10^{10.5} - 10^{10.9} M_\odot$ central stellar mass bin. At higher central mass bins, simulations tend to slightly have more satellites than the observations at the lowest mass ends. Hence overall, the total number of satellites is in broad agreement, with a hint that MUFASA underproduces the satellite population at intermediate masses ($\sim 10^{10} M_\odot$).

In contrast, we see more substantial discrepancies when examining the satellite GSMFs broken down by quiescent vs. star-forming. At the lowest central masses, most satellites are blue (star-forming), and MUFASA reproduces those well. However, MUFASA strongly over-predicts the (small) number of red satellites, particularly at the lowest satellite masses. At higher central masses, the observed red satellite mass function is relatively shallow (thick red dashed lines), albeit with an upturn at the lowest masses, whereas MUFASA predicts a steeper red satellite GSMF. Particularly, for the most massive centrals, MUFASA predicts that red satellite galaxies dominate at all masses, while in Tal et al. (2014) they only dominate at $M_* \gtrsim 10^{10.5} M_\odot$.

The overall redshift evolution predicted in MUFASA is qualitatively consistent with that seen by Tal et al. (2014), where they used three redshift bins such as (0.2, 0.5), (0.5, 0.85) and (0.85, 1.20). For illustration, we only show the simulated sample at $z = 0.25$ (thin solid lines) and $z = 1$ (dotted lines) which span the redshift ranges used in their sample. The star-forming satellite mass functions show very little evolution with time, with a hint of being slightly higher at higher redshift. They dominate the mass function at low masses, and are more prevalent at earlier epochs. Meanwhile, there is a mild increase with time for the quenched satellite population, but the trend with mass is much more significant; there is a much larger number of red satellites per group around massive centrals, and at high masses they dominate over the star-forming satellites. These general trends are qualitatively in agreement with the observations. However, as noted before, MUFASA strongly overproduces the number of low-mass red satellites, at essentially all central masses. Moreover, MUFASA tends to grow massive red satellites more rapidly than the low-mass red satellites,

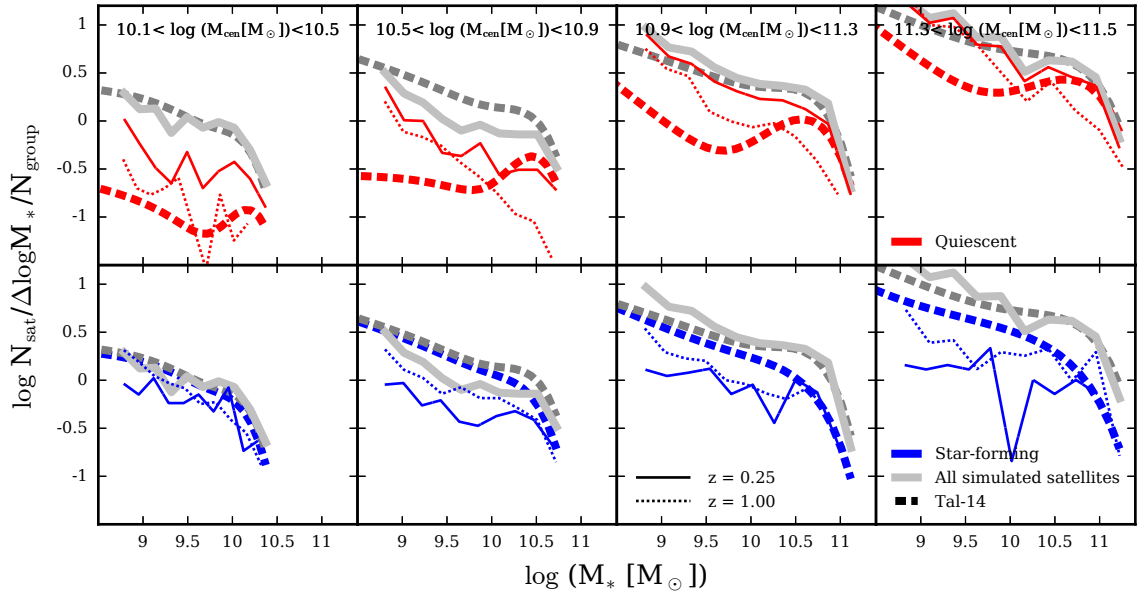


Figure 4. Satellite galaxy stellar mass functions (thick grey lines, $z = 0$); separated into star forming (lower panels, blues) and quenched (upper panels, reds) population. We show them at two different redshift $z = 0.25$ (thin solid lines), and $z = 1$ (thin dotted lines). The thick dashed lines show the double-Schechter fits from Tal et al. (2014, see Table 1): blue for star forming, red for quenched and gray for all satellites.

which is opposite to what is seen in the data in which the most massive satellites are already in place fairly early on.

Several avenues could lead to these discrepancies. For instance, MUFASA identifies central galaxies via a 3-D friends-of-friends scheme, while in Tal et al. (2014), centrals are identified as having no other more massive system within two projected virial radii, which can blend systems in projection. In particular, it could be that the “bump” of massive red satellites identified by Tal et al. (2014) are actually nearby massive central galaxies. Furthermore, Tal et al. (2014) must do substantial background subtraction to count satellites, which can be uncertain particularly when low numbers of satellites are present. We could in principle mimic the first selection effect, but the second effect would require detailed modeling of the background population, which is beyond the scope of this work. In general, without a more careful mimicking of the observational selection effects, the significance of these discrepancies is not completely clear.

If we take the discrepancies at face value, it suggests that MUFASA over-quenches satellites in haloes of all masses, particularly low masses satellites. This is consistent with the findings in Davé et al. (2017a), but here we see this across a range of mass bins and epochs. The discrepancy for high-mass centrals may owe to the extreme nature of our quenching mechanism, where we keep gas hot all the way out to the virial radius. For low-mass centrals, however, the quenching mechanism is not obviously relevant, except if such low-mass centrals happen to be in the vicinity of high-mass centrals (“neighbourhood quenched”; Gabor & Davé 2015). Hence the discrepancies may reflect details of hydrodynamic processes, or else some of the systematic effects mentioned in the previous paragraph. For now, we will consider the broad agreement as sufficient for examining galaxy conformity in

MUFASA, with the caveat that MUFASA does not well reproduce the low-mass satellite population when broken up by colour.

3.3 Halo-centric satellite colours

Conformity was first specified as a commonality in colours between nearby centrals and satellites. Hence an important aspect to investigate in our models is the colours of satellite galaxies as a function of radius. In this section we examine the halo-centric colours of satellite galaxies.

Figure 5 shows $g - r$ contour plots of all satellites in MUFASA, as a function of radius scaled by the virial radius R_{vir} . The red shaded area shows the quiescent satellites, while the star-forming satellites are depicted by the blue shaded area; we remind the reader that these are divided at $\text{sSFR} = 10^{-2.2} \text{ Gyr}^{-1}$. The right y-axis histograms show the colour distributions of the satellites: blues (reds) for star forming (quiescent) satellites at $r < 0.5R_{\text{vir}}$, and cyan (magenta) for star forming (quiescent) satellites at $r \geq 0.5R_{\text{vir}}$. We show for three different halo mass bins. As a test of numerical convergence, we also show the colour distributions of our $25h^{-1} \text{ Mpc}$ box in thin histograms on the left y-axis.

We can see a strong bimodality distribution in terms of colour that extends out to the virial radius. This bimodality exists for all halo masses, although the relative number of red and blue satellites changes substantially with halo mass. There are a few dusty star-forming satellites that have red colours lying underneath the red contour, but these are small fraction of the total. The strong bimodality in colour was first noted observationally by Kauffmann et al. (2003); Balogh et al. (2004), and is interpreted to indicate that satellite galaxies quench fairly rapidly once the quenching process begins (e.g. Wetzel et al. 2015). MUFASA broadly

reproduces these observed trends. The thin histograms from the $25h^{-1}\text{Mpc}$ volume along the left y-axis are qualitatively similar, although the bimodality is somewhat weaker maybe because the smaller volume does not produce as many massive quenched systems and the model performs differently at that resolution.

Examining the trends with halo size, we clearly see a decrease of star forming population towards larger halo masses. For less massive haloes, we see that quiescent satellites are mostly located at the core (inner $\sim 10 - 15\%$) of the groups while the star forming satellites are almost evenly distributed. For intermediate-mass haloes, the star forming satellites inside $< 0.5R_{\text{vir}}$ rarify and the quiescent galaxies extend out to $\geq 0.5R_{\text{vir}}$. For the most massive haloes, only the satellite galaxies at the very edge of the haloes are forming stars. These trends are again qualitatively consistent with observations, as more massive central galaxies tend to be quenched and have more environmentally-quenched satellites (e.g. Peng et al. 2012).

Overall, these results taken together generally indicate that the satellite population in MUFASA qualitatively reproduces observations, including the satellite population evolution split by red versus blue galaxies. The most notable discrepancy is that MUFASA predicts an excess of low-mass red satellites in massive haloes. Broadly, this is expected to strengthen the conformity of red centrals with red neighbours in massive haloes, hence the predicted conformity is likely to be overestimated in this regime. Modulo this caveat, MUFASA provides a fairly viable platform to study the radial distribution of galaxy properties around central galaxies.

4 CONFORMITY IN $s\text{SFR}$, HI RICHNESS AND COLOUR OF THE GALAXIES.

Traditionally, galaxy conformity is known as the tendency for central galaxies and their satellites to have similar colours (Weinmann et al. 2006). However, conformity could in principle be associated with any galaxy property. For instance, conformity has recently been quantified in neutral hydrogen (Kauffmann et al. 2013), with central and satellite galaxies found to be similar in their HI richness. One could equivalently define conformity between different galaxy properties. For example, one could quantify by how much blue central galaxies have higher HI satellites, or quantify how older central galaxies have lower $s\text{SFR}$ satellites. We will call this *cross-conformity*, differentiated from *auto-conformity* (or just, conformity).

In this section, we examine galaxy conformity in MUFASA in terms of colour, HI content and $s\text{SFR}$. We also make predictions for cross-conformity among these properties. Here we will take bins of central galaxy stellar mass in order to be able to compare to observations particularly of Kauffmann et al. (2013), but we forego a detailed matching of selection for particular samples that can be critical for proper quantitative interpretation (as discussed in §1). Instead, we focus on the nature and strength of conformity as predicted in MUFASA.

Using the approach of Kauffmann modulo our definition of central galaxies, the closest neighbours are satellites, representing one-halo conformity, and those farther out are other haloes' central and satellite galaxies representing two-

halo conformity. Hence for each neighbour property, we generate a plot of three mass bins, which we show in columns, and three central galaxy properties, which we show as rows. We will consider conformity in the neighbour properties of colour, $s\text{SFR}$ and HI richness; thus we have three such plots.

Figure 6 shows the first of these plots, depicting the $g-i$ colour of the neighbouring galaxies as a function of projected distance to their respective centrals R_{proj} . The error bars are from jackknife resampling. The top row represents traditional conformity: the tendency for neighbouring galaxies to share the colour of their central galaxy. The median colour of central galaxies in the top and bottom quartiles of colour are shown as the values in the upper right, for each mass bin. The values at the bottom right of the bottom panels show the number of central galaxies for each stellar mass bins (color coded, where the normal (bold) fonts are for m25n512 (m50n512)). The thick lines show our fiducial box (m50n512), but we also show our smaller (higher resolution) box (m25n512) with the thin lines for comparison. The vertical dotted lines (colour coded) show the median values of the virial radii of the central galaxies with 1σ uncertainties shown towards the bottom of each panel. We show the plot out to $R_{\text{proj}} = 4 \text{ Mpc}$, beyond which point we will later show the conformity signal essentially disappears in all tracers.

In the lowest mass bin, conformity is evident at all scales; the central galaxies have a median $g-i = 0.83$ magnitudes, and the neighbours tend to have a similar colour all the way out to 4 Mpc. The colour of the bluest quartile of centrals is $g-i = 0.25$, but here the neighbours are generally redder than the central, with $g-i \approx 0.6 - 0.7$; nonetheless they are still clearly bluer than the neighbours of red centrals.

The intermediate and high-mass bins show conformity as well, but restricted only to within $R_{\text{proj}} \lesssim 1-2 \text{ Mpc}$, with a trend for less extended conformity in larger galaxies. The conformity is also relatively weak, as the colour difference in the neighbours is $\lesssim 0.2$ magnitudes, while the colour difference between the centrals in the highest and lowest quartiles is much larger, $\sim 0.5 - 0.7$.

Thus MUFASA clearly shows evidence for colour-colour conformity. While it weakens with projected distance, it still extends well beyond R_{vir} , and thus we predict two-halo conformity to exist albeit with a strength that rapidly diminishes with radius. We will quantify the strength of conformity in §5. It could be that the two-halo conformity reflects only backplash satellites whose orbit takes them beyond the nominal virial radius, or neighbourhood-quenched galaxies (Gabor & Davé 2015); we will investigate the nature of these galaxies in detail in future work.

The middle row shows the level of colour conformity when selecting central galaxies by HI fraction. Cross-conformity between HI richness and colour is equivalently evident as for colour-colour (auto-)conformity. Here, at low masses the cross-conformity only extends to $\sim 2 \text{ Mpc}$, which is similar to what is seen at intermediate masses.

Finally, in the bottom panel, we show the cross-conformity between $s\text{SFR}$ and colour. For an extinction-free stellar population, these two would essentially be identical. We have included extinction in computing our colours, so the similarity in trends with the colour-colour conformity is not completely trivial, but nonetheless the trends do look quite

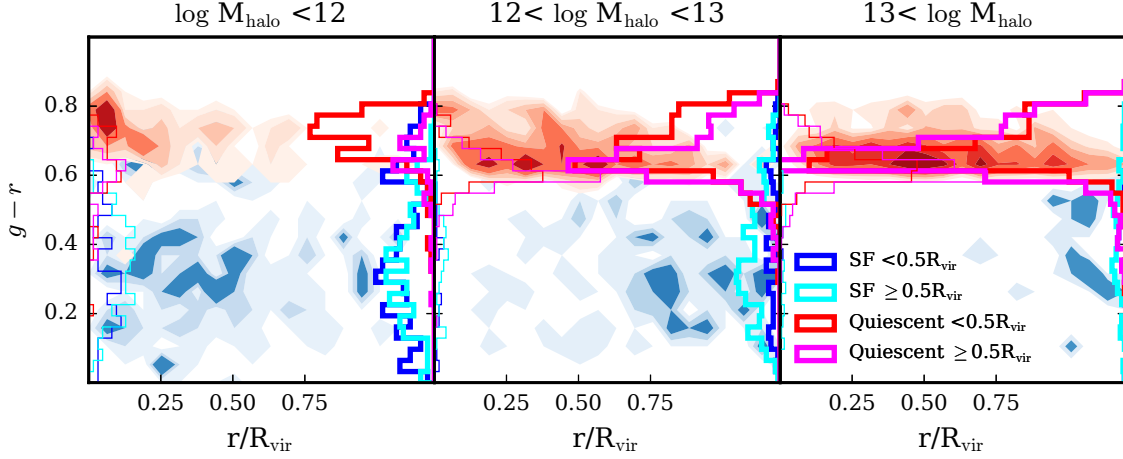


Figure 5. $g-r$ colour of neighbouring galaxies depending on their distances to the centre of their corresponding haloes ($z=0$). The red (blue) shaded area shows the distribution of the quiescent (star forming) satellites in our simulated sample. The histograms along the right y-axes show the distribution of the satellites depending on their specific star formation rate and their distance to the halo centers. We also show the colour distributions of our smaller box (higher resolution, but poorer statistics) on the left y-axes.

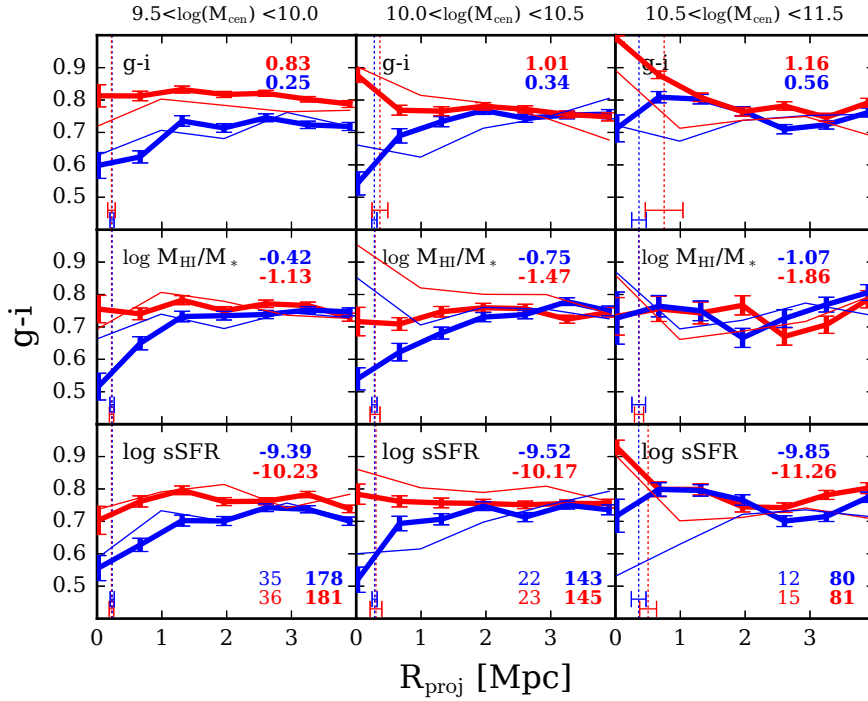


Figure 6. Median $g-i$ colours of galaxies as a function of projected distances around central galaxies divided in three stellar mass bins (columns). Within each stellar mass bins, the red/blue curves denote the median colours of galaxies around the upper/lower quartiles of central galaxies in $g-i$ (top panels), HI richness (middle panels), and sSFR (bottom panels). The median values of each quartiles of the central galaxies are shown on top of each panel. The number of central galaxies in each stellar mass bins are shown on the bottom right of the bottom panels: the lower (upper) quartile is in red (blue) (normal font: m25n512, bold font: m50n512). The thick lines show our fiducial box (m50n512) and the thin lines our smaller (higher resolution) box (m25n512). The errorbars are estimated with jackknife resampling. The vertical dashed lines show the median values of the R_{vir} of the hosts of the central galaxies (colour coded), with the errorbars at the bottom left quantifying the standard deviation. The top row represents the conformity signal in $g-i$, while the bottom two rows represent the cross-conformity of centrals' HI richness and sSFR with satellites' $g-i$.

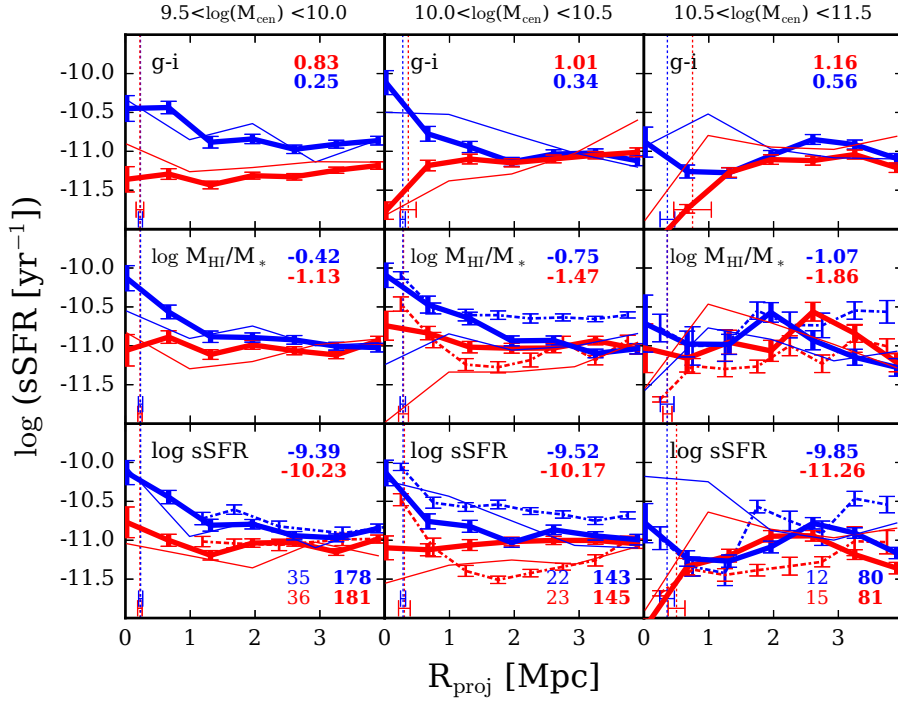


Figure 7. Similar to 6, except showing the sSFR of the neighbours. Dashed lines (colour coded) show SDSS observations from Kauffmann et al. (2013) and Kauffmann (2015) for reference, with the caveat that we have not mimicked their selection in detail.

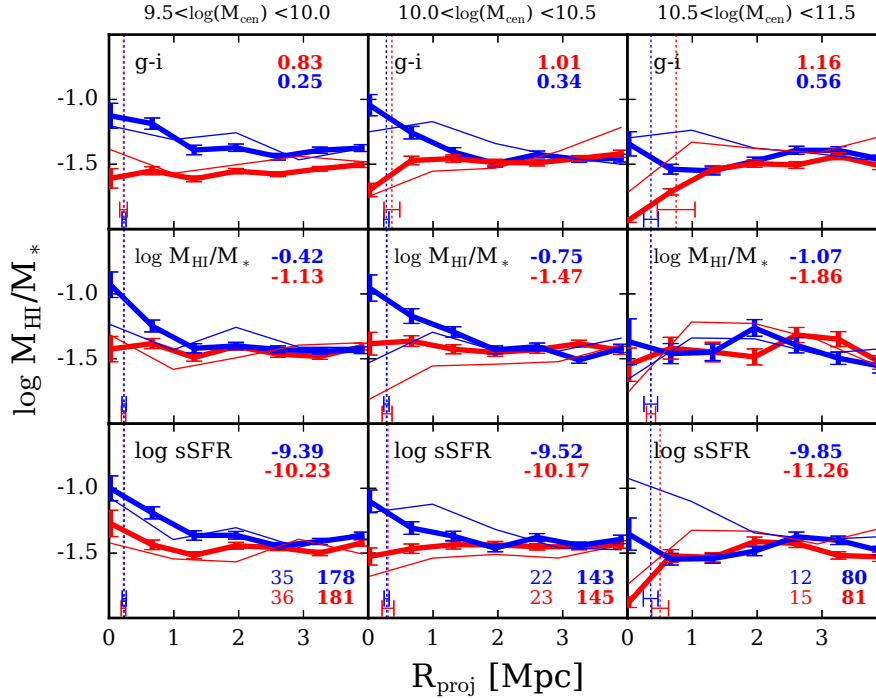


Figure 8. Similar to 6, except showing the HI richness of the neighbours.

similar. As such, herein we will primarily consider sSFR as a proxy for colour.

An interesting note is that for low and intermediate mass galaxies, the bluest, most HI-rich, or most star-forming galaxies all have close neighbours that are significantly bluer than faraway neighbours. However, in the most massive bin, this turns around, and the satellite colours become redder moving in from $R_{\text{proj}} \lesssim 1$ Mpc. The trend in colour is also present but somewhat weaker than in sSFR, since it is partially offset by decreasing extinction from the lower gas content at small radii. This shows the strong effect that our halo-based quenching model has on truncating the gas content and star formation in satellite galaxies.

In Figure 7, we show conformity in the sSFR's of neighbouring galaxies. The trends are quantitatively similar to that seen in the colour conformity case, except flipped in sign since higher colours correspond to lower sSFR. Again, conformity is seen out to ~ 2 Mpc in lower-mass galaxies, and is strongly radial dependent. Here, we can see that the sSFR conformity clearly increases at low separations for HI and sSFR, for low and intermediate mass galaxies.

Conformity has been measured in SDSS with respect to sSFR (Kauffmann et al. 2013) and HI (Kauffmann 2015). These data are shown as the dashed lines in the lower two rows. The median values of the simulated galaxy properties are in reasonable agreement with the observed trends. At low and intermediate central masses, the amplitude of the separation between the top and bottom quartiles are in agreement with data at $R_{\text{proj}} \lesssim 1$ Mpc, and also show an increase of neighbours' sSFR to small separations. For the largest masses, the upturn at small radii in neighbour colour, HI content, and sSFR is not as strong, and this again is in broad agreement with observations. We emphasise that our isolation criterion based on using only central galaxies in friends-of-friends haloes is not the same as that used in (Kauffmann et al. 2013). As we showed in Figure 2 there are only mild differences between these different isolation criteria and strongest only for the most massive centrals, and thus it is instructive to compare to the (Kauffmann et al. 2013) data even if the criteria are not identical. Meanwhile, our results provide predictions that are more comparable to recent group catalog-based analyses such as that of Tinker et al. (2017).

In detail, at intermediate masses the observed neighbours of lowest-quartile centrals become substantially higher (bluer) at small separations, while MUFASA does not predict this trend (though the agreement is good for highest-quartile centrals). One explanation for this discrepancy could be that mergers increase sSFR at low separations, but this enhancement is not properly reflected in the simulations, perhaps owing to resolution. At larger radii, the data continues to show strong conformity that is not seen in MUFASA, but these data are somewhat in doubt owing to interloper contamination as discussed in Sin et al. (2017); Tinker et al. (2017). Our results are broadly in agreement with the semi-analytic or abundance matching models presented in those works, for which conformity disappears at distances not far beyond the virial radius in more massive galaxy samples.

For completeness, we consider in Figure 8 the conformity trend in the HI richness of neighbours, for central galaxies split by colour (top row), HI richness (middle), and sSFR (bottom). The trends generally mimic those in

the other cases, in that conformity is only detectable out to $R_{\text{proj}} \lesssim 2$ Mpc, and is only strong at $R_{\text{proj}} \lesssim 1$ Mpc. The neighbours' HI richness, like colour and sSFR, becomes higher (bluer) towards small separations for low-mass centrals, but become lower (redder) for high-mass centrals.

Comparing the $50h^{-1}$ Mpc (thick) and $25h^{-1}$ Mpc (thin) line predictions, we see that in general the conformity signature is qualitatively similar at both resolutions, though they are not within each others' formal error bars. As shown in Davé et al. (2017b), the two volumes are not completely converged in terms of many of their stellar and gas properties. Ironically, the convergence in conformity strength appears to be best-converged for the smallest centrals; at higher masses, the trends are less well mimicked in the two volumes, though overall the trends are similar. On top of the rather small sample from m25n512, we also speculate that the discrepancy might also be from the model behaving differently at different resolutions. We note that the error bars for the $25h^{-1}$ Mpc results (not shown for clarity) are generally larger than for the $50h^{-1}$ Mpc.

Overall, MUFASA displays fairly strong galaxy conformity within $\lesssim 1$ Mpc projected radius, and weak conformity in most cases out to ~ 2 Mpc, which disappears at high masses. The conformity signature is present and similar in all permutations of central vs. neighbour galaxy properties considered here, namely colour, HI richness, and sSFR. The trend to small radius at large central masses shows the impact of halo quenching, but for lower central masses we see bluer, more gas rich, and higher sSFR neighbours towards small radii. Comparing to observations of Kauffmann et al. (2013); Kauffmann (2015), the trends generally agree at projected radii less than about 1 Mpc. MUFASA does not produce as strong conformity at larger scales as inferred by those data, but at large separations these data may be impacted by interloper contamination. Observational comparisons are sensitive to details of selection effects etc. particularly at large radii, so we consider the outcome of conformity in MUFASA and the broad agreement at $R_{\text{proj}} \lesssim 1$ Mpc to be encouraging, and leave a more detailed data comparison for future work.

5 THE NATURE OF CONFORMITY

In the previous section we showed that galactic conformity is present in MUFASA in specific star formation rate, HI richness, and colour of galaxies at similar levels, with conformity being stronger at small separations and extending farther out in lower-mass central galaxies. Physically, one might regard conformity as a reflection of quenching processes associated with hot massive haloes (e.g. Peng et al. 2012; Gabor & Davé 2015). MUFASA assumes a quenching halo mass scale of $\sim 10^{12} M_{\odot}$, and hence the effects of conformity might be expected to be stronger in haloes above this mass scale, since the gas surrounding satellites has now been forcibly heated to the virial temperature. However, starvation and stripping processes can happen in lower-mass haloes through tidal interactions and harassment. Hence it is an interesting question to quantify how conformity changes with halo mass, particularly across our quenching mass threshold.

To this end, in this section we subdivide our sample with respect to halo mass above and below our nominal quenching

scale, as opposed to subdividing in stellar mass as in the previous section in order to more closely compare with data. Furthermore, we consider conformity in a wider range of properties beyond only what has been observed, to a more exhaustive set of galaxy properties. This will help us identify which properties display the strongest conformity, and hence in some sense drive galactic conformity.

5.1 Conformity in non-quenched haloes

Figure 9 shows, from top to bottom panels, the sSFR (yr^{-1}), f_{HI} (HI richness), f_{H_2} (molecular hydrogen fraction), Z (gas phase metallicity), Age (median value of the stellar ages, in Gyr) and Σ_3 (third projected nearest neighbour density) of central galaxies in haloes of $\log(M_{\text{halo}}/M_{\odot}) < 12$, ordered by each of those properties (columns). The trends for sSFR and f_{HI} were shown in Figure 7 and Figure 8 binned by central stellar mass, but here we show them binned by halo mass. The diagonal panels (from lower left to upper right) show the (auto-)conformity in each quantity, while the off-diagonals show the cross-conformity with the rows representing the neighbour properties and the column representing the central properties.

Before we delve into a detailed analysis, it's important to keep in mind the nature of galaxies in this halo mass bin. Note that the median sSFR of the reddest quartile of central galaxies is $\log(\text{sSFR}/\text{Gyr}^{-1}) = -1.23$, which is not a quenched galaxy by our (or almost any reasonable) definition. This is not surprising, since in MUFASA, we do not apply our quenching prescription in this range of halo masses. Nonetheless, it is worth bearing in mind that here we are mostly examining trends among star-forming galaxies, subdivided into redder vs. bluer, more gas-rich versus less, etc. Since there exist trends with galaxy mass in these quantities (e.g. Davé et al. 2017b), binning in these quantities implicitly includes some trend with galaxy mass. Ideally, one would remove this effect by sub-binning in narrow bins of galaxy (or halo) mass, but given our statistics, this is not feasible.

Let us consider the auto-conformities first, along the diagonal panels. For all quantities except Z , the conformity is well-defined out to remarkably large scales, exceeding the 4 Mpc (projected) limit that we consider here, with a strength that diminishes relatively slowly. We also saw this behavior in some but not all cases around the low-mass centrals shown in Figures 6-8. This implies that neighbours know about their large-scale environment out to quite large distances. This likely does not reflect halo (AGN) quenching, ram pressure stripping, or other processes traditionally associated with massive haloes, since it is not confined near the haloes themselves, nor are the selected massive haloes. Instead, it represents conformity driven by the growth of large-scale structure by the tendency for massive galaxies (with e.g. redder colours and lower gas content) to live around other massive galaxies.

The most striking trend is seen in the first column of Figure 9. Here, we see that the difference between the satellite properties is always greatest when the centrals are subdivided by our environment measure Σ_3 . This is true not only for the Σ_3 auto-conformity but for every cross-conformity measure as well. From this, we conclude that the most important driver of conformity is the nearby galaxy

density, and clearly identifies galactic conformity in low-mass haloes as environmentally-driven. This is perhaps unsurprising, since conformity is inherently itself a tracer, i.e. if galaxy properties vary smoothly with environment, then having many galaxies of a similar type close to each other will give rise to strong signals in both Σ_3 and galaxy conformity.

The next strongest level of difference between satellite quartiles is provided by separating centrals in stellar age (second column from left). This is qualitatively consistent with the findings of Hearin et al. (2016), who argued that assembly bias is crucial for driving two-halo conformity. Although we have restricted this sample to $M_{\text{halo}} < 10^{12} M_{\odot}$, it is possible that the environmental dependence of the halo mass function within this mass range may drive conformity, with the age aspect being a consequence rather than a driver (Zu & Mandelbaum 2017); this would be consistent with our results that the environment shows the strongest trend in conformity. To test this, we would need to construct an age-matched sample within each environment, but unfortunately given our limited simulation volume, the results are too noisy to extract clear trends.

We next examine the gas and star formation rate conformity properties. Interestingly, the conformity signature is at least as strong when centrals are subdivided by f_{H_2} , as compared to either sSFR or f_{HI} . This is notable since current observations have mainly probed the latter two (since they are the most observationally accessible given current data), but MUFASA predicts that these conformity signals are actually similar if not weaker compared to that seen in molecular gas fractions.

Finally, the metallicity has a very minor conformity signal, only at $R_{\text{proj}} < 1$ Mpc. The most curious aspect is that qualitative trend in the metallicity of neighbours relative to the sSFR. Looking at the top row of the metallicity column, then at low R_{proj} , one sees that low- Z centrals tend to have neighbours with slightly higher sSFR. This is consistent with the fundamental metallicity relation (e.g. Mannucci et al. 2010; Lara-López et al. 2010), where at a given mass, galaxies with high sSFR have low- Z and vice versa; this trend is reproduced in MUFASA (Davé et al. 2017b), and apparently extends to satellites as well. In contrast, if you look at the sSFR (6th) column, fourth panel down, it curiously shows that centrals with high sSFR are surrounded by neighbours with *high* metallicity – in other words, the trend is flipped, and metallicity actually shows anti-conformity! The differences are subtle but robust, which we will quantify later on. This may arise as an age effect – one can see in the Age (2nd) column, fourth panel down, that galaxies with young ages tend to be much more metal-rich, because they have had longer time to form stars and hence enrich themselves.

In general, we note that the overall amplitude of conformity looks most similar in the columns of our plot, rather than in the rows. This means that the conformity is generally most driven by the *central* galaxy property being examined, but relatively independent of the neighbour property being examined. In contrast, the trends with radius are most similar when examining a particular neighbour galaxy property.

The physical interpretation of one-halo conformity in non-quenched haloes likely traces back to halo assembly bias. This is because, in this regime, there is no explicit physics that will turn nearby galaxies red, as there is in the

quenched haloes case where there is strong local quenching feedback. Hence the similarity of galaxy colours likely arises owing to the tendency for haloes living in denser regions to have formed earlier and be surrounded by more gravitationally shock-heated gas, which results in an overall reduction of the accretion rates onto all galaxies living in such extended structures. This is essentially a form of assembly bias, in which galaxies at a given halo mass experience different growth histories depending on their large-scale assembly history. Such an interpretation is consistent with that of Tinker et al. (2017) from SDSS and Bray et al. (2016) from examining the origin of conformity in the Illustris simulation.

In summary, $M_{\text{halo}} < 10^{12} M_{\odot}$ haloes show noticeable conformity across almost all galaxy properties, with the strongest absolute differentiations among neighbours occurring in environment (Σ_3). Specific SFR, f_{HI} and Age have actually rather weak conformity signal relative to that, and somehow comparable to molecular fraction f_{H_2} . There is little conformity in galaxy metallicities, and in fact shows opposite trends depending on whether one considers cross-conformity versus the central's metallicity or the neighbour's metallicity. Some of these trends may arise owing to mass trends among central galaxies when binned into upper and lower quartiles. We will discuss conformity more quantitatively in §5.

5.2 Conformity in quenched haloes

We now conduct a similar investigation, but for centrals within quenched haloes having $M_{\text{halo}} \geq 10^{12} M_{\odot}$. Figure 10 shows the analogous plot to Figure 9 for these quenched haloes. Note that the typical sSFR of upper-quartile centrals is only a factor of 2 lower than in the low-mass halo case, but for lower-quartile centrals the sSFR is more than an order of magnitude lower, showing the onset of a considerable quenched population in massive haloes. Similarly, the magnitude of the difference is substantially larger between the highest and lowest quartile in gas content as well.

The trends at high halo masses are clearly different than for the lower mass haloes examined in the previous section. Most strikingly, conformity in just about every property is now restricted only to $R_{\text{proj}} \lesssim 1 - 1.5$ Mpc, with the exception of Σ_3 . Within that range, the radial trend is much stronger than in the low-mass halo case, as quenching clearly plays a role in impacting the satellite galaxy population. The one-halo conformity is obviously well stronger than the two-halo conformity, showing that satellites in particular are very strongly impacted by environmental-specific processes owing to quenching.

Looking at individual properties, we see once again that environment (Σ_3) shows the strongest absolute levels of conformity, and its auto-conformity extends out to ~ 4 Mpc. The cross-conformities tend to nearly vanish beyond $\gtrsim 2$ Mpc. But in contrast to the low-mass halo case, the strengths and radial trends of the conformities in other properties are remarkably similar, and even the metallicity shows strong conformity.

These trends show qualitatively the behaviour one would expect, with centrals that are high-sSFR, gas-rich, young, and low-density having like neighbours. The exception again is metallicity, where low- Z centrals tend to have

high- Z satellites and neighbours, and vice versa. The anti-conformity of metallicity is an interesting testable prediction.

Recall that in §3.2 we highlighted an issue with these simulations in that they overproduce the number of low-mass quenched satellites. This is expected to increase the 1-halo conformity term for the reddest (and analogously least star-forming and gas-rich) quartile, since quenched central galaxies are also red. The magnitude of this effect is difficult to quantify without a new feedback model that is able to mitigate this discrepancy. We are currently working on such a model, but do not have final results at this time. For now, we note that the quenched halo predictions may change depending on the new input physics required to fix this discrepancy.

In summary, both low-mass and high-mass (quenched) haloes show conformity in virtually all quantities, but the trends are qualitatively different. High-mass haloes show a relatively confined (spatially) extent of conformity, with a very strong radial trend, and similar conformity strength in all properties except for Σ_3 which is the strongest. In the next section we discuss our approach to quantifying these trends, in order to more carefully inter-compare and study their evolution with redshift.

5.3 Quantifying conformity

Previous works have generally focused on quantifying conformity by measuring its detectable radial extent, within a given tracer. The next logical step would be to quantify the conformity strength in a manner such that we can inter-compare the strengths among various tracers. In the previous sections, we have focused on comparing the *absolute* strength of conformity within a given neighbour property, binned by central property. However, it is not obvious how to compare this strength between different properties, since effectively this absolute conformity signal (say, the difference between the red and blue curves) has units associated with that property. Thus we need a new a measure that also enables cross-comparisons between various neighbour properties, in order to more robustly determine which neighbour property shows the strongest conformity.

The fundamental idea of conformity is to quantify how well the neighbours follow the trends of their central. In this sense, a good measure of conformity to inter-compare properties would be to measure the difference between the neighbour properties, relative to how much difference there is in the central galaxy properties. This may be regarded as a *relative* conformity, as opposed to the absolute conformity that we have investigated in the previous sections. As such, we define (relative) conformity strength \mathcal{S} as follows:

$$\mathcal{S} = \frac{1}{N_{\text{bin}}} \sum_{i=0}^{N_{\text{bin}}-1} \frac{Q1_i - Q4_i}{Q1_{\text{cen}} - Q4_{\text{cen}}} \quad (5)$$

where $Q1_{\text{cen}}$ ($Q4_{\text{cen}}$) is the property of the central galaxies in the 1st (4th) quartile, $Q1_i$ ($Q4_i$) is the (logarithm of the) property of the galaxies neighbouring the 1st (4th) quartile in the radial bin i . In this way, we normalize the difference in neighbour properties by the difference in the central property. Generally, we will consider $\mathcal{S}(R < 2 \text{ Mpc})$, i.e. summing

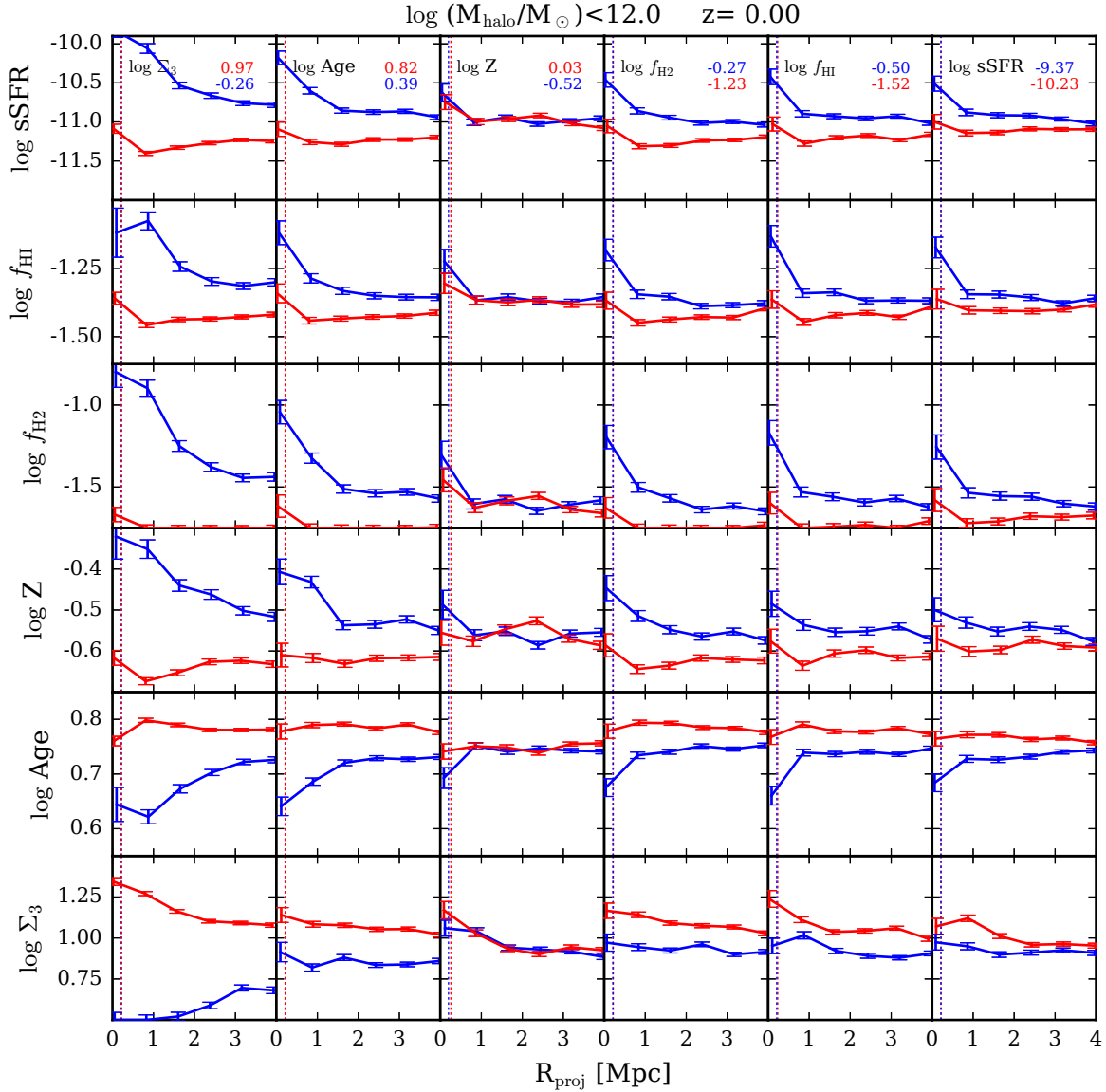


Figure 9. Neighbour galaxy median properties versus projected distance to their central galaxies living in haloes with mass $M_{\text{halo, cen}} < 10^{12} M_{\odot}$, binned by central galaxies in highest and lowest quartile for each given property. The specific property shown in each column is indicated in the upper left of the top row, while the median quantities for the central galaxies are indicated on the upper right (color coded with the lines). The dashed vertical lines are the median values of the R_{vir} of the central galaxies in the highest and lowest quartiles.

all bins that are within 2 Mpc of the central galaxy. We will also consider $\mathcal{S}(R)$, i.e. taking a single bin at each radius.

Broadly, $\mathcal{S} = 1$ means that the neighbours show exactly the same difference between the top and bottom quartiles as the centrals; this is full conformity. $\mathcal{S} = 0$ means no conformity. We will characterise weak conformity as $\mathcal{S} < 0.5$, and strong above this. It is possible to get $\mathcal{S} > 1$ which indicates very strong conformity, with neighbours showing a greater difference in a property than even their centrals, or even $\mathcal{S} < 0$ which is anti-conformity. Hence this quantity provides an intuitive measurement of conformity that is independent of the given property. We note that this is not a new definition of conformity. We use similar definition of

conformity from [Kauffmann et al. \(2013\)](#) but only extend it to be presentable in one number.

5.4 Conformity as a function of mass and radius

In Figure 11, we show $\mathcal{S}(R < 2 \text{ Mpc})$ at $z = 0$ for central galaxies binned by their halo masses: we chose each bins to contain the same number of central galaxies. Σ_3 signal shows the strongest conformity signal, quantifying the trend in the previous sections that conformity is most strongly related to environment. The Σ_3 conformity is however anti-correlated with halo mass, so environment is the primary driver at low and intermediate halo masses, but at the highest halo masses it is comparable to the other quantities. While we discussed

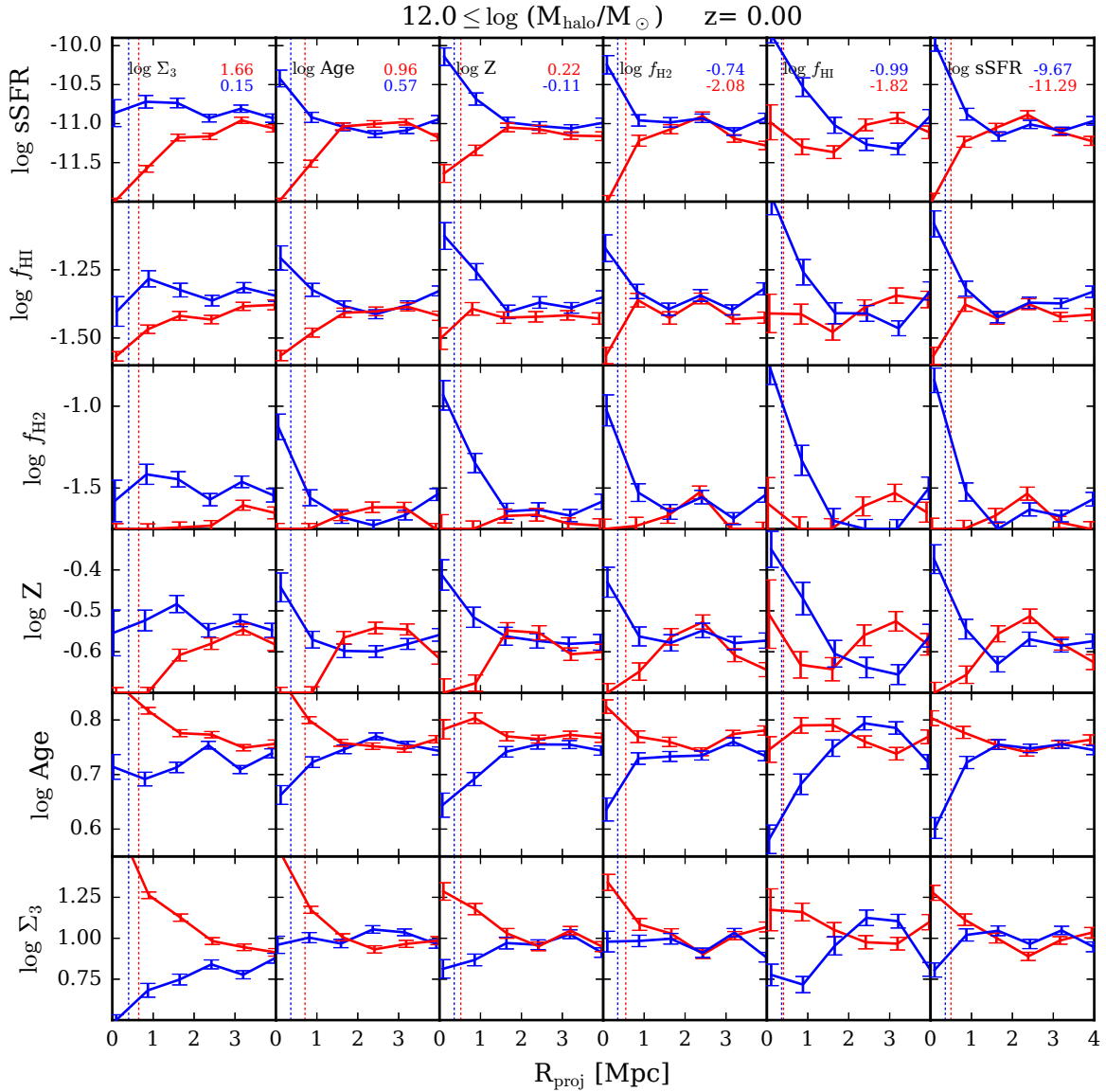


Figure 10. Similar to Figure 9 except for centrals living in $M_{\text{halo,cen}} \geq 10^{12} M_{\odot}$.

previously that this perhaps not surprising since conformity corresponds to the similarity in properties of nearby galaxies, while Σ_3 is itself a measure of how many nearby galaxies there are, it is not a trivial result, since it indicates that galaxies that lie particularly close to each other in dense regions have similar properties. Moreover, the trend with mass is interesting, and is driven by the difference between the central galaxy properties, i.e. the denominator of \mathcal{S} , increasing. Hence, effectively, large-scale structure is the primary driver of conformity when quenching processes are not present, but once they are, then it is no longer so dominant.

Besides Σ_3 , sSFR clearly shows the strongest conformity at most halo masses. Recall that in the previous section we found that Age and f_{H_2} were stronger in an absolute sense. However, when computing \mathcal{S} , we normalize this to the difference in the central galaxy property, and in this case we discover that sSFR conformity is stronger than that of

Age, f_{H_2} , or f_{HI} . Thus it appears that, beyond the obvious dependence of conformity on environment, sSFR shows the strongest levels of similarity between the neighbours and the central galaxies. Though we do not show it here, we expect galaxy colour would show a very similar trend to sSFR, as we found in §4.

As discussed previously, metallicity shows anti-conformity at most halo masses, increasingly so to larger halo masses. Recall this is the SFR-weighted gas-phase metallicity, not the stellar metallicity; one might expect a different trend for stellar metallicity, as central galaxies within large haloes tend to have metal-rich stars but their star-forming gas may be dominated by recent infall that is relatively metal-poor.

Observational analyses from, e.g., Tinker et al. (2017); Sin et al. (2017) suggest that galactic conformity is only prevalent in the relatively nearby environment, within \lesssim

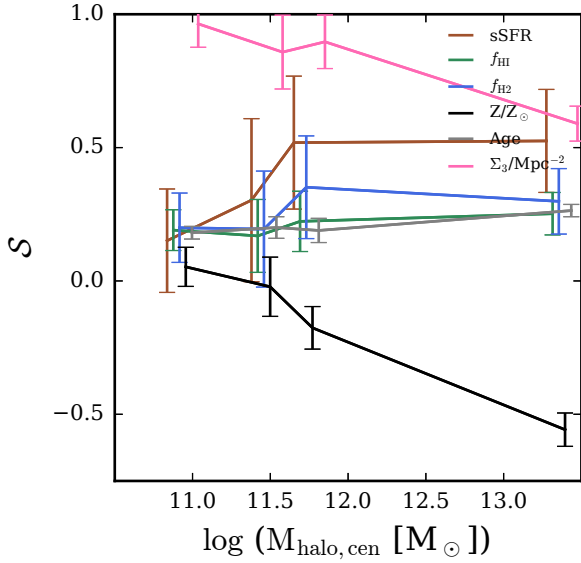


Figure 11. Halo mass dependence of the auto-conformity strength in MUFASA at redshift $z = 0$. Halos have been binned so that each bin contains approximately the same number. 1σ error bars are derived by jackknife resampling. Environment shows the strongest conformity at low masses, but gets weaker with halo mass. sSFR shows the strongest conformity among the remaining quantities, and increases with halo mass from $M_{\text{halo}} \sim 10^{12} M_{\odot}$. Metallicity displays anti-conformity.

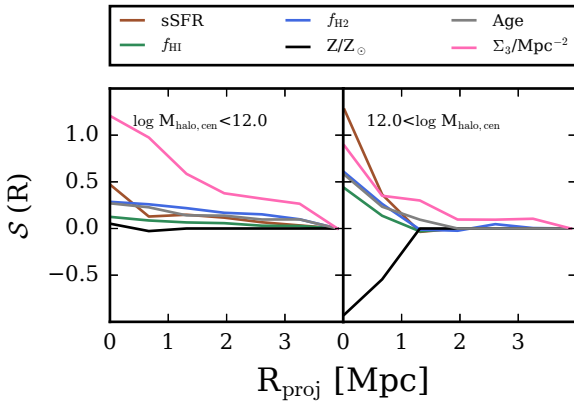


Figure 12. Radial dependence of conformity strength $S(R)$. Here S is computed within each radial bin. Low-mass haloes show weak conformity with little radial trend, except for Σ_3 . Massive haloes show stronger conformity for neighbours close to the central, but little conformity at $R_{\text{proj}} > 1$ Mpc.

1 Mpc. It can be seen in Figure 10 that, particularly in massive haloes, that were generally the targets of these studies, the conformity signal predicted in MUFASA drops quickly with radius. However, this is less true in low-mass (non-quenched) haloes (Figure 9), which shows overall weaker conformity but much less radial dependence.

To quantify this, we show in Figure 12 the conformity signal as a function of projected radius R_{proj} , for non-quenched (left panel) and quenched (right) haloes. The qualitative trends evident in Figures 9 and 10 are evident here.

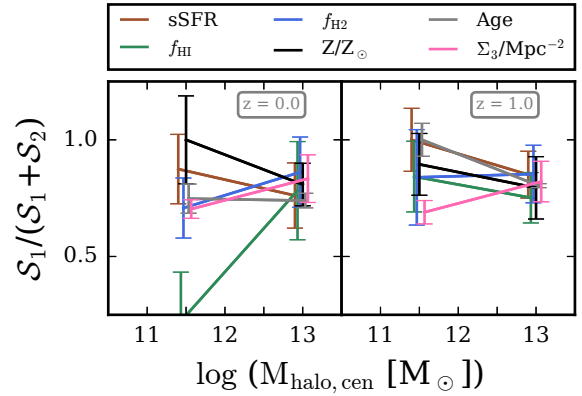


Figure 13. Halo mass evolution of the relative contribution of the one-halo conformity. S_1 (S_2) is one(two)-halo conformity. One-halo conformity generally dominates the signal for all quantities except HI in low-mass haloes.

The conformity is strongest in the environmental measure Σ_3 at all radii, except close in for massive haloes. Conformity is relatively weak with modest radial dependence in the low-mass haloes, while it is strong at $R < 1$ Mpc in the massive haloes but mostly nonexistent beyond this (except in Σ_3). In fact, in the innermost bin, the sSFR shows stronger conformity that even Σ_3 , exceeding unity. It is thus perhaps not surprising that conformity was first noticed for colours of satellites around sizeable galaxies (Weinmann et al. 2006) – MUFASA predicts the conformity signal is quite strong under these conditions.

In summary, conformity is strongest in environment, confirming the environmental nature of galaxy conformity. Beyond this, the next strongest conformity is in sSFR, which is mildly stronger than gas fraction and Age. Metallicity presents an odd anti-conformity particularly in quenched haloes, which may be a signature of recent accretion of metal-poor star-forming gas into massive central galaxies. Massive haloes show a strong conformity signal in most quantities only at $\lesssim 1$ Mpc, while less massive haloes show a weaker conformity with a weaker gradient.

5.5 One-halo vs. two-halo conformity

A particularly interesting quantity to examine is the relative contribution of one-halo versus two-halo conformity to the total conformity signal, as there has been substantial debate in the literature regarding the strength, origin, and even existence of two-halo conformity. Here we explicitly examine this for each halo, computing only the conformity associated with galaxies that are satellites within the haloes of the chosen central, versus those outside the halo up to 2 Mpc. Note that this is not a strict radial cut, since FOF haloes typically have non-spherical shapes.

Figure 13 shows the fractional contribution of one-halo conformity (S_1) versus two-halo (S_2), specifically $S_1/(S_1+S_2)$, as a function of halo mass. Owing to small number statistics for the one-halo term particularly at low halo masses, we separate our central galaxy sample into only two bins of halo mass, $M_{\text{halo}} < 10^{12} M_{\odot}$ and $M_{\text{halo}} \geq$

$10^{12} M_{\odot}$. The left panel shows the $z = 0$ results, while the right shows $z = 1$.

It is clear that one-halo conformity dominates the overall strength for almost all quantities for both low and high mass haloes, at both $z = 0$ and $z = 1$. The only deviant case is the HI fraction in low mass haloes, which likely owes to the physical effect that satellite galaxies around star-forming centrals can have their HI stripped relatively easily, so that such centrals actually end up having different HI fraction relative to their satellites but more similar to distant galaxies. Typically, one-halo conformity is $\sim 3-6\times$ stronger than two-halo conformity, according to our \mathcal{S} measure. We note that while the strength of one-halo conformity dominates in most circumstances, the strength of two-halo conformity at small radii depends on halo mass, and this may be partly the cause of divergent results in the literature regarding two-halo conformity.

5.6 Evolution of conformity

Conformity has been observed to exist out to $z \gtrsim 1$ and beyond, although the strength of the evolution is difficult to quantify at this time. In this section we examine the evolution of conformity strength \mathcal{S} predicted by MUFASA.

There are two ways to track the conformity back in time for a galaxy population. One way is to find the conformity strength for the most massive progenitors of the $z = 0$ central galaxies; we will call this $\mathcal{S}_{\text{track}}$, since we are tracking individual galaxies. Another way is to consider the centrals in the same halo mass bins as at $z = 0$, separated at $M_{\text{halo}} = 10^{12} M_{\odot}$; we will call this \mathcal{S}_{ev} , which shows the overall evolution of conformity. In both cases we take the absolute value $|\mathcal{S}(< 2 \text{ Mpc})|$ for plotting purposes, and note that only the metallicity shows negative values (anti-conformity).

Figure 14 shows the evolution of galactic auto-conformity strength, (i.e. quantifying the diagonal panels of Figures 9 and 10), for central galaxies binned into two halo mass ranges: $\log(M_{\text{halo}}/M_{\odot}) < 12$ and $12 < \log(M_{\text{halo}}/M_{\odot})$. For clarity of the plot, we set the strength to 0 when \mathcal{S} crosses 0 and stay on the other side of the 0-line for two successive snapshots. In addition, we smoothed the curves to their moving averages over $\Delta z = 0.1$ for $z < 0.5$, and 0.2 elsewhere, to average over the fluctuations among individual redshift snapshots.

The left panels show $\mathcal{S}_{\text{track}}$ (top) and \mathcal{S}_{ev} (bottom) for low mass (unquenched) haloes. For these, conformities are generally weak at all redshifts. Tracking our specific central galaxies back from $z = 0$, f_{HI} and Z emerge earlier than the others at $z \sim 1$, while the others only appear at $z < 0.25$. Because these are small haloes, we are limited in how far back we can track these galaxies before they lack resolution to follow. However, it is evident that we can track sufficient numbers till at least $z \sim 1$, so it is interesting that the low-mass conformity we see at $z = 0$ in many quantities is actually quite a late-time phenomena for these particular galaxies. This suggests that conformity in e.g. Σ_3 or sSFR requires halo masses that approach $\sim 10^{12} M_{\odot}$, and at significantly smaller halo masses there is no conformity except the metallicity anti-conformity. With larger statistical samples from upcoming larger-volume simulations, we will be able to test this idea more finely.

Examining \mathcal{S}_{ev} for low-mass haloes, we see that confor-

mity is very uniform and weak at all redshifts, with the exception of Σ_3 as noted before. Again, this suggests that there is mass threshold for the emergence of conformity that is close to $\sim 10^{12} M_{\odot}$. There is a hint that conformity strength increases with time for a fixed halo mass sample, but given the small statistics at $z \gtrsim 2$ it is difficult to draw firm conclusions.

Turning to the high mass haloes (right panels), we see much stronger levels of conformity in some quantities. In particular, in $\mathcal{S}_{\text{track}}$ (top right) sSFR conformity is extremely strong out to $z \gtrsim 2$. Hence for massive haloes, even tracking them back in time shows that classic (colour-based) conformity emerges quite early on. We note that this trend is driven by a few massive haloes that have a large number of satellites, since conformity in massive haloes is generally restricted to relatively small radii and hence are dominated in statistics by satellites. This also causes some odd behaviour such as the Age- $\mathcal{S}_{\text{track}}$ which spikes up around $z \sim 1$; we hesitate to over-interpret this behavior without more statistics. It is also the case, as at lower masses, that gas conformity is a relatively late-time phenomenon, appearing only at $z \lesssim 1$.

For \mathcal{S}_{ev} in high-mass haloes, again we see that the conformity strength is fairly constant with redshift. The metallicity (anti-)conformity shows the most significant increase with time. This is consistent with the idea that conformity in most quantities is primarily driven by environment (which correlates strongly with halo mass), except for metallicity where the anti-conformity is driven by a different effect namely the late infall of low-metallicity gas into massive galaxies.

Another way to quantify conformity is to ask, how far from the central galaxy should we expect conformity to be evident? To quantify this, we measure the distance from the central galaxies where the two-halo conformity still exists (R_2), relative to the mean R_{vir} of the central galaxy subsample. R_2 is measured as the largest projected distance from the central galaxies where the highest and lowest quartile samples are first within 1σ of each other (e.g. where the blue and red lines are within each other's error bars in Figure 9). We note that R_2 is thus mildly sensitive to the level of the error bars, and hence the sample size.

In Figure 15 we show R_2 as a function of redshift for low (left panels) and high (right) halo mass bins and tracked either using progenitors (top panels) or at a fixed halo mass bin (bottom), analogous to Figure 14.

At $z = 0$ for small haloes, we see as in Figure 9 that the conformity extends out to many virial radii; we truncate this at 2 Mpc, corresponding to ≈ 18 median virial radii in that halo mass bin. However, tracking these galaxies back in time shows that the conformity radius disappears extremely rapidly, with the exception of HI fraction for which it extends to $z \sim 2$. Even using a fixed halo mass bin, R_2 starts dropping beyond $z \gtrsim 0.25$, and disappear by $z \sim 1$.

For massive haloes, R_2 extends typically out to $\sim 5R_{\text{vir}}$, as long as it is present. Tracking galaxies back, we see that when conformity emerges, it emerges quickly to this radius. Of course, this exact radius as well as the exact redshift depend on the sample size, but the trend of rapid emergence is robust. When looking within a fixed halo mass bin, we see the radius to which noticeable conformity extends is remarkably constant out to $z \sim 2$ in terms of typical virial radii.

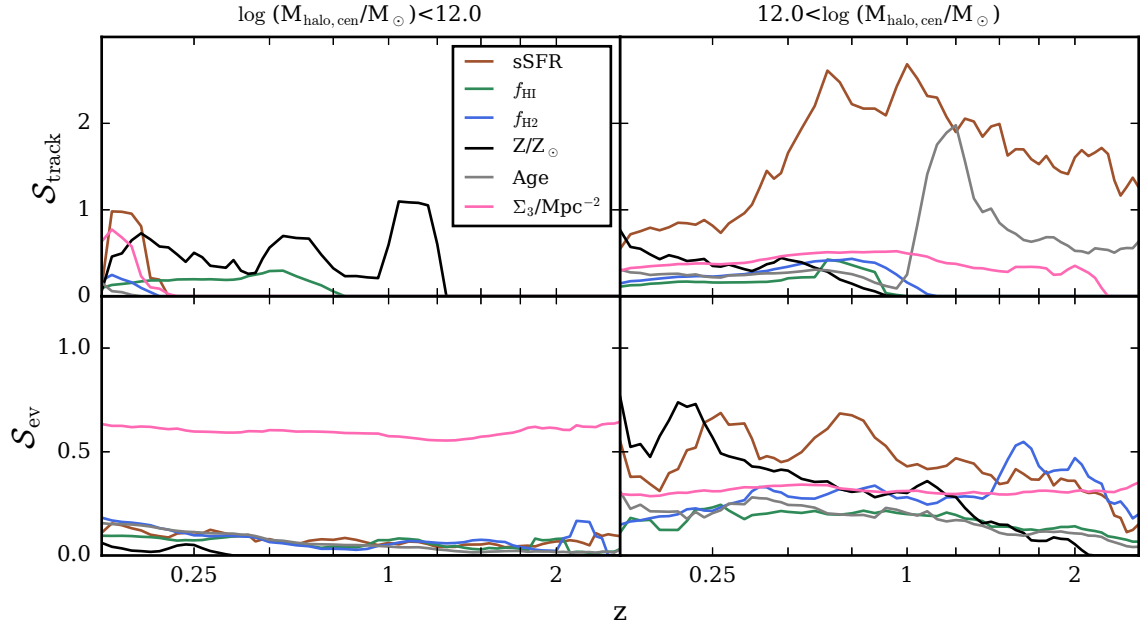


Figure 14. Evolution of the strength of galactic conformity. The halo mass range of the central galaxies are given on top of the columns. Upper panels show the evolution the conformity strengths tracking back the $z = 0$ progenitors in time. Lower panels show the evolution of conformity within the listed halo mass bins at each redshift independently. Conformity is a late-time emergent phenomenon more associated with high-mass haloes, suggesting that it is dependent on quenching physics.

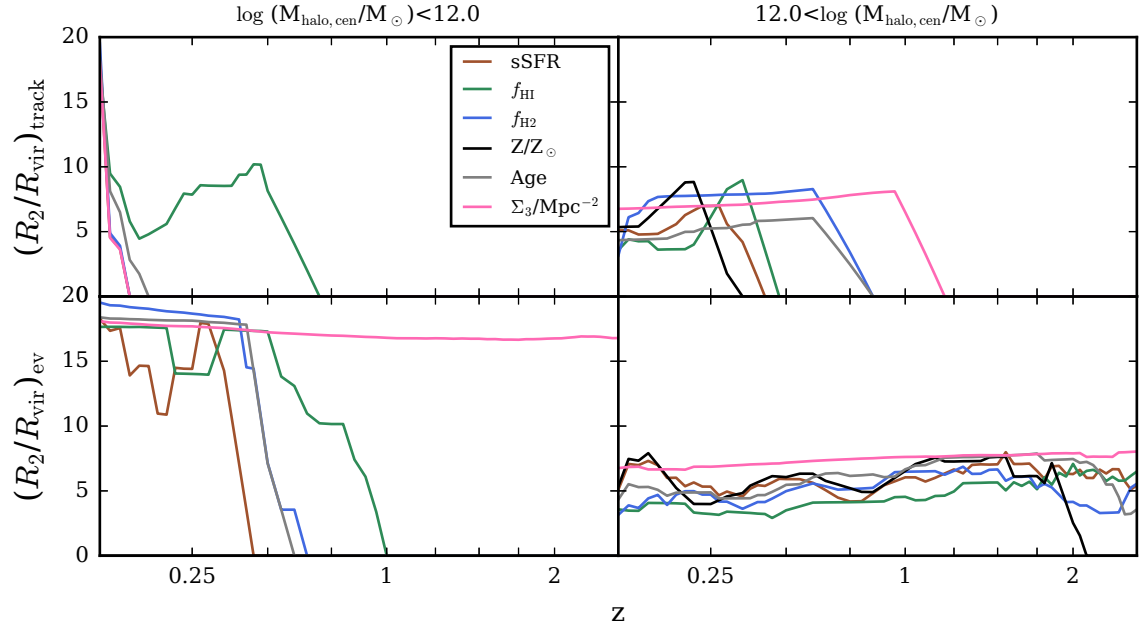


Figure 15. Extent of the two-halo conformity. R_2 is the distance from the primary galaxies to the point where the two-halo conformity still exists, i.e blue and red lines in Figure 9 are within each other's error bars. At low masses, conformity emerges at late epochs and quickly to large numbers of virial radii. At high masses, once it appears, conformity is evident out to a fairly constant $\sim 5R_{\text{vir}}$.

In summary, conformity in low-mass haloes appears to be a late-time effect, likely arising from haloes as they approach $\sim 10^{12}M_{\odot}$. Tracking massive haloes, conformity is evident and strong in sSFR at all redshifts, but in the gas properties and stellar age it is relatively weak and emerges

at $z \lesssim 1$. When looking at $> 10^{12}M_{\odot}$ haloes at each redshift, conformity is fairly constant in terms of both strength as well as number of radii to which it extends. Hence we predict that conformity should be evident in reasonably massive galaxies at approximately the same level at higher redshifts

as at $z = 0$. These trends are qualitatively consistent with observations showing that conformity continues to be evident out to $z \sim 2$.

6 SUMMARY & CONCLUSION

We have examined galaxy conformity as an emergent property of a cosmological hydrodynamic simulation of galaxy formation. In particular, we employ the MUFASA simulation that has been shown to reasonably reproduce a range of observed galaxy physical properties over much of cosmic time (Davé et al. 2016, 2017b). The approach for quenching massive galaxies in this simulation is purely heuristic, utilising a slowly-evolving threshold halo mass above which diffuse halo gas is prevented from cooling, which well reproduces the observed red/blue bimodality in the galaxy population (Davé et al. 2017a) but does not invoke a specific physical model driving the quenching. Galaxy conformity provides a relatively unexplored statistic with which to quantify how such quenching impacts the properties of galaxies in various environments. To this end, we examine conformity in galaxy properties that have been previously looked at in the literature, namely colour, HI fraction and specific SFR, along with a range of other galaxy properties such as molecular content, stellar age, gas-phase metallicity, and environmental density.

Our main findings are as follows:

- MUFASA yield approximately the observed fraction of total satellite galaxies as a function of central galaxy mass. However, it overproduces the low-mass quenched satellites, most noticeably around high mass central galaxies when the quenched satellite dominate the count (Figure 4).

- Satellite galaxy colours are generally bimodal for all halo masses and radii, with quenched satellites at small radii and star-forming ones farther out. The transition radius between these varies with central mass: $< 10^{12} M_{\odot}$ haloes have quenched satellites dominating only within the inner 10-15% of R_{vir} , while $> 10^{13} M_{\odot}$ haloes have star-forming satellites primarily in the outer 10-15% (Figure 5).

- Very broadly, galaxy conformity is evident in MUFASA at all stellar masses examined ($M_{*} > 10^{9.25} M_{\odot}$), in essentially all quantities examined. It typically extends significantly beyond the virial radius, though the strength diminishes with radius (Figures 6, 7, 8).

- Focusing on conformity in $g-i$ colour, specific star formation rate (sSFR) and HI, we find that conformity at low (central) galaxy mass is relatively weak, compared to high mass galaxy, but extends to quite large radii, while conformity at high galaxy mass declines more quickly with radius. The cross-conformity among these three quantities show similar trends to the (auto-)conformity (Figures 6, 7, 8).

- We subdivide our galaxies into “unquenched” ($M_h < 10^{12} M_{\odot}$) and “quenched” ($M_h > 10^{12} M_{\odot}$) haloes, which provides a more direct view of the impact of quenching on neighbouring galaxies. Low-mass haloes show relatively weak conformity compared to high-mass haloes, extending to large radius, likely arising from assembly bias by which galaxies residing in more dense environments experience earlier growth and more suppression of accretion today. Meanwhile, high-mass haloes show conformity rapidly declining

with radius and typically disappearing at projected radii above ~ 1 Mpc. This strong qualitative difference demonstrates that the presence of a sustained hot halo in our model has a major impact in driving strong galaxy conformity in our simulation (Figures 9, 10).

- Qualitatively, the strength of the conformity or cross-conformity signal is most directly correlated with the central galaxy property being examined, while the radial trend of the (cross-)conformity signal is dependent on the neighbour property. Environment (as measured by the density to the third nearest projected neighbour) and stellar age appear to have the largest absolute (cross-)conformity signals, while metallicity shows a very small signal. The conformity strength in sSFR, f_{HI} , and f_{H2} are comparable (Figures 9, 10).

- We introduce a measure $\mathcal{S}(R)$ (where R is the projected radius) to quantify the conformity strength, defined as the difference in the neighbour galaxies’ properties in the first and fourth quartiles relative to that of the central galaxies. By normalizing to the central galaxies, this constructs a dimensionless “relative” conformity strength that can be used to inter-compare different properties. $\mathcal{S}(R)$ is unity if the neighbours show as much difference as centrals, while it is zero if they show no difference, and can be negative if the satellites’ difference is in the opposite sense to the centrals’.

- $\mathcal{S}(R < 2\text{Mpc})$ is strongest for environment, but this strength declines with halo mass. Low-mass ($M_h \sim 10^{11} M_{\odot}$) haloes show very weak conformity ($\mathcal{S} \sim 0.1-0.2$) in all quantities, but for sSFR and f_{H2} this rises to moderate strengths ($\mathcal{S} \sim 0.3-0.5$) by $M_h \sim 10^{12} M_{\odot}$. Age and f_{HI} always show relatively weak conformity. Metallicity, interestingly, shows increasing anti-conformity ($\mathcal{S} < 0$) with halo mass, possibly owing to the increasing number of satellites coupled with the reduced gas-phase metallicity in centrals from small amounts of fresh accretion (Figure 11).

- Consistent with qualitative impressions, $\mathcal{S}(R)$ for low-mass haloes is weak but present at all R in most quantities, while in massive haloes it is strong at small radii but declines rapidly and vanishes at $R \gtrsim 1$ Mpc. At the smallest radius, i.e. for satellite galaxies, $\mathcal{S}(R)$ is strongest for sSFR (or equivalently galaxy colour), and even in low-mass haloes this declines relatively quickly with R (Figure 12).

- For quantities that show significant conformity, $\mathcal{S}(R)$ is dominated by one-halo conformity over two-halo. An exception to this is for f_{HI} in small haloes, where small satellites of gas-rich centrals can get their neutral gas stripped, resulting in more similarity in this quantity with neighbours farther out (Figure 13).

- Tracking conformity back in time for the $z = 0$ galaxy population, we find that conformity is a late-time phenomenon for low-mass haloes for all properties except metallicity. Massive haloes develop conformity earlier, and the sSFR conformity is generally always the strongest, with \mathcal{S} significantly exceeding unity at intermediate redshifts. These trends are consistent with the idea that significant conformity only occurs once halo start to be quenched (Figure 14).

- Tracking conformity within fixed halo bins at all redshifts, we find that conformity strength is fairly constant, with low-mass haloes always showing very weak conformity and high-mass haloes showing stronger conformity (Figure 15).

- Our conformity results are generally qualitatively but

not quantitatively consistent between our fiducial simulation and our $25h^{-1}$ Mpc volume with $8\times$ better resolution, in part due to the different performance of the model at different resolutions. In fact, at our fiducial resolution, our feedback model appears to overproduce low-mass quenched satellites (Figure 4), particularly in quenched haloes. It is likely that part of the strong one-halo conformity signal in our massive haloes arises from such over-quenched satellites.

Overall, galaxy conformity appears to be a generic prediction of models that quench massive galaxies approximately in accord with observations. However, the strength, extent, and dependence on specific property are all likely to depend significantly on the precise physical model driving the quenching. In our case, we have tested a heuristic but observationally-consistent scenario where the hot gas in massive haloes is kept hot, which yields concordant central galaxy properties, and showed that it has a substantial impact on galaxy conformity developing in massive haloes. This provides a new approach to testing quenching models by examining neighbouring galaxies, as opposed to tests that focus on the properties of the central galaxies or their surrounding gas. It remains to be seen what the impact of a more physically-motivated quenching prescription using energy released from AGN would have on conformity; this will be explored in future work. This paper presents a first step towards quantifying conformity in a way that will allow observations to be compared to models more stringently, and thereby potentially provide a new way to constrain AGN feedback in modern galaxy formation models.

ACKNOWLEDGEMENTS

The authors thank G. Kauffmann for providing us with the observational data and useful ideas for this work, as well as helpful suggestions from the referee. The authors also thank F. Durier and T. Naab for helpful conversations and guidance. MR and RD acknowledge support from the South African Research Chairs Initiative and the South African National Research Foundation. MR acknowledges financial support from Max-Planck-Institut für Astrophysik. Support for MR was also provided by the Square Kilometre Array post-graduate bursary program. The MUFASA simulations were run on the Pumbaa astrophysics computing cluster hosted at the University of the Western Cape, which was generously funded by UWC's Office of the Deputy Vice Chancellor. Additional computing resources are obtained from the Max Planck Computing & Data Facility (<http://www.mpcdf.mpg.de>).

REFERENCES

- Ann H. B., Park C., Choi Y.-Y., 2008, *MNRAS*, **389**, 86
- Baldry I. K., Glazebrook K., Brinkmann J., Ivezić Ž., Lupton R. H., Nichol R. C., Szalay A. S., 2004, *ApJ*, **600**, 681
- Baldry I. K., et al., 2012, *MNRAS*, **421**, 621
- Balogh M. L., Baldry I. K., Nichol R., Miller C., Bower R., Glazebrook K., 2004, *ApJ*, **615**, L101
- Berti A. M., Coil A. L., Behroozi P. S., Eisenstein D. J., Bray A. D., Cool R. J., Moustakas J., 2016, preprint, ([arXiv:1608.05084](https://arxiv.org/abs/1608.05084))
- Bigelow B. C., Dressler A. M., 2003, in Iye M., Moorwood A. F. M., eds, Proc. SPIE Vol. 4841, Instrument Design and Performance for Optical/Infrared Ground-based Telescopes. pp 1727–1738, [doi:10.1117/12.461870](https://doi.org/10.1117/12.461870)
- Birnboim Y., Dekel A., 2003, *MNRAS*, **345**, 349
- Bray A. D., et al., 2016, *MNRAS*, **455**, 185
- Conroy C., Gunn J. E., 2010, FSPS: Flexible Stellar Population Synthesis, Astrophysics Source Code Library (ascl:1010.043)
- Croton D. J., et al., 2006, *MNRAS*, **367**, 864
- Davé R., Thompson R., Hopkins P. F., 2016, *MNRAS*, **462**, 3265
- Davé R., Rafieferantsoa M. H., Thompson R. J., 2017a, preprint, ([arXiv:1704.01135](https://arxiv.org/abs/1704.01135))
- Davé R., Rafieferantsoa M. H., Thompson R. J., Hopkins P. F., 2017b, *MNRAS*, **467**, 115
- Faucher-Giguère C.-A., Kereš D., Dijkstra M., Hernquist L., Zaldarriaga M., 2010, *ApJ*, **725**, 633
- Gabor J. M., Davé R., 2012, *MNRAS*, **427**, 1816
- Gabor J. M., Davé R., 2015, *MNRAS*, **447**, 374
- Gabor J. M., Davé R., Finlator K., Oppenheimer B. D., 2010, *MNRAS*, **407**, 749
- Geha M., Blanton M. R., Yan R., Tinker J. L., 2012, *ApJ*, **757**, 85
- Hahn O., Abel T., 2011, *MNRAS*, **415**, 2101
- Hartley W. G., Conselice C. J., Mortlock A., Foucaud S., Simpson C., 2015, *MNRAS*, **451**, 1613
- Hatfield P. W., Jarvis M. J., 2016, preprint, ([arXiv:1606.08989](https://arxiv.org/abs/1606.08989))
- Hearin A. P., Watson D. F., van den Bosch F. C., 2015, *MNRAS*, **452**, 1958
- Hearin A. P., Behroozi P. S., van den Bosch F. C., 2016, *MNRAS*, **461**, 2135
- Hopkins P. F., 2015, *MNRAS*, **450**, 53
- Kauffmann G., 2015, *MNRAS*, **454**, 1840
- Kauffmann G., et al., 2003, *MNRAS*, **341**, 33
- Kauffmann G., Li C., Zhang W., Weinmann S., 2013, *MNRAS*, **430**, 1447
- Kawinwanichakij L., et al., 2016, *ApJ*, **817**, 9
- Kennicutt Jr. R. C., 1998, *ApJ*, **498**, 541
- Kereš D., Katz N., Weinberg D. H., Davé R., 2005, *MNRAS*, **363**, 2
- Klypin A. A., Trujillo-Gomez S., Primack J., 2011, *ApJ*, **740**, 102
- Krumholz M. R., Gnedin N. Y., 2011, *ApJ*, **729**, 36
- Lara-López M. A., Bongiovanni A., Cepa J., Pérez García A. M., Sánchez-Portal M., Castañeda H. O., Fernández Lorenzo M., Pović M., 2010, *A&A*, **519**, A31
- Lawrence A., et al., 2007, *MNRAS*, **379**, 1599
- Mannucci F., Cresci G., Maiolino R., Marconi A., Gnerucci A., 2010, *MNRAS*, **408**, 2115
- McCracken H. J., et al., 2012, VizieR Online Data Catalog, **354**
- McNamara B. R., Nulsen P. E. J., 2007, *ARA&A*, **45**, 117
- Mitra S., Davé R., Finlator K., 2015, *MNRAS*, **452**, 1184
- Moster B. P., Naab T., White S. D. M., 2013, *MNRAS*, **428**, 3121
- Muratov A. L., Keres D., Faucher-Giguere C.-A., Hopkins P. F., Quataert E., Murray N., 2015, ArXiv e-prints:1501.03155,
- Oppenheimer B. D., Davé R., Kereš D., Fardal M., Katz N., Kollmeier J. A., Weinberg D. H., 2010, *MNRAS*, **406**, 2325
- Peng Y.-j., Lilly S. J., Renzini A., Carollo M., 2012, *ApJ*, **757**, 4
- Planck et al., 2016, *A&A*, **594**, A13
- Rahmati A., Schaye J., 2014, *MNRAS*, **438**, 529
- Schmidt M., 1959, *ApJ*, **129**, 243
- Sin L. P. T., Lilly S. J., Henriques B. M. B., 2017, preprint, ([arXiv:1702.08460](https://arxiv.org/abs/1702.08460))
- Somerville R. S., Davé R., 2015, *ARA&A*, **53**, 51
- Springel V., 2005, *MNRAS*, **364**, 1105
- Straatman C. M. S., et al., 2014, *ApJ*, **783**, L14
- Tal T., Quadri R. F., Muzzin A., Marchesini D., Stefanon M., 2014, preprint, ([arXiv:1405.4856](https://arxiv.org/abs/1405.4856))
- Tinker J. L., Hahn C., Mao Y.-Y., Wetzel A. R., Conroy C., 2017, preprint, ([arXiv:1702.01121](https://arxiv.org/abs/1702.01121))
- Tomczak A. R., et al., 2014, *ApJ*, **783**, 85

- Vogelsberger M., et al., 2014, ArXiv e-prints:1405.2921,
Voit G. M., 2005, *Advances in Space Research*, **36**, 701
Wang J., et al., 2015, *MNRAS*, **453**, 2399
Weinmann S. M., van den Bosch F. C., Yang X., Mo H. J., 2006,
MNRAS, **366**, 2
Wetzel A. R., Tollerud E. J., Weisz D. R., 2015, *ApJ*, **808**, L27
White S. D. M., Rees M. J., 1978, *MNRAS*, **183**, 341
York D. G., et al., 2000, *AJ*, **120**, 1579
Zu Y., Mandelbaum R., 2017, preprint, ([arXiv:1703.09219](https://arxiv.org/abs/1703.09219))